TÂNIA SOFIA DE SOUSA MAGALHÃES NETO

Master Thesis

Development of an injectable self-assembled bioactive hybrid hydrogel

Dissertação submetida ao Instituto de Ciências Biomédicas Abel Salazar da Universidade do Porto para obtenção do grau de Mestre em Biotecnologia Molecular

Doutora Isabel Freitas Amaral (supervisor)

Doutor Pedro M.D. Moreno e Doutora Victoria Leiro (co-supervisor)

2018

This work was performed at:

i3S – Instituto de Investigação e Inovação em Saúde, Universidade do Porto
INEB – Instituto de Engenharia Biomédica, Universidade do Porto, Portugal

The research described in this thesis was financially supported by: projects NORTE-01-0145-FEDER-000008 and NORTE-01-0145-FEDER-000012, financed by Norte Portugal Regional Operational Programme (NORTE 2020), under the PORTUGAL 2020 Partnership Agreement, through the European Regional Development Fund (ERDF), and FEDER funds through the COMPETE 2020 - Operacional Programme for Competitiveness and Internationalisation (POCI), and by National Funds through FCT/MCTES in the framework of the project "Institute for Research and Innovation in Health Sciences" (POCI-01-0145-FEDER-007274).

“There's always going to be bad stuff out there. But here's the amazing thing – light trumps darkness, every time. You stick a candle into the dark, but you can't stick the dark into the light.”

Jodi Picoult

Agradecimentos

Antes de mais, gostaria de agradecer a todas as pessoas envolvidas no meu trabalho, mas, em particular, à minha orientadora Isabel Amaral por ter sido incansável ao longo deste período, por estar sempre disponível para me ajudar sempre que duvidava do meu trabalho, por acreditar sempre nas minhas capacidades e me ter ensinado tanto em tão pouco tempo!

A todo o nBTT e, em especial à Doutora Ana Paula Pêgo, por me ter recebido de braços abertos e por ter acreditado em mim ao longo deste percurso.

Ao Pedro Moreno e à equipa do UP3, Frederico Silva e Fátima Fonseca, por me terem ajudado a compreender novas técnicas e explicado, mais do que uma vez, os conceitos, até garantirem que eu entendia todo o trabalho.

Sem nunca me esquecer deles, agradeço também aos meus pais, Helena e Miguel, por me terem dado todo o apoio que precisei para conseguir terminar o curso, dando-me a mão e limpando-me as lágrimas quando parecia que nada funcionava. Aos meus irmãos, Cláudia e Dinis, por compreenderem quando não podia brincar ou sair com eles porque tinha que estudar, por saberem que, independentemente de tudo, serão sempre das pessoas mais importantes para mim. A toda a minha família, muito obrigada! Sem vocês nada disto teria significado. Ao meu namorado, Bruno, por entender todo o meu stress e por me deixar descarregar a frustração nele sempre que algo corria mal. Foram os meus pilares e ajudaram-me sempre que os obstáculos pareciam demasiado grandes para ultrapassar.

Não esquecendo também os meus amigos fantásticos, antigos e recentes, que apoiaram o meu percurso e me ajudaram a dar sempre o melhor do mim. Obrigado por todas as gargalhadas que partilhamos. Levo-vos no coração!

Agradeço, naturalmente, a todos os que me dedicaram o seu tempo, que me ajudaram, que me fizeram lutar por isto e que me inspiraram!

Simplesmente, obrigada!

Table of contents

Abbreviation List

2D/3D	Two-dimensional/Three-dimensional
ACN	Acetonitrile
A-SH	Thiol adenine
BBB	Blood-Brain barrier
bFGF	Basic fibroblastic growth factor
BM-MSC	Bone marrow-derived mesenchymal stem cell
BSA	Bovine serum albumin
CLSM	Confocal laser scanning microscopy
CNS	Central nervous system
DAPI	4',6-Diamidino-2-phenylindole
DNA	Deoxyribonucleic acid
DTNB	Ellman's reagent
DTT	Dithiothreitol
ECM	Extracellular matrix
ESC	Embryonic stem cell
F-actin	Filamentous actin
Fb	Fibrin
G'	Storage modulus
G''	Loss modulus
HA	Hyaluronic acid
hESC	Human embryonic stem cell
hES-NSC	hESC-derived neural stem cell
hES-NSPC	hESC-derived neural stem progenitor cell
HPLC	High-performance liquid chromatography
iNSC	Induced neural stem cells
iPSC	Induced pluripotent stem cell
LVER	Linear viscoelastic region
MAL	Maleimide
MITCH	Mixing-induced two-component hydrogel
NSC	Neural stem cell
NSPC	Neural stem/progenitor cell
OEC	Olfactory ensheathing cell
Pa	Pascal
PAGE	Polyacrylamide gel electrophoresis

PBS	Phosphate buffered saline
PEG	Poly(ethylene glycol)
PEG-MAL	Maleimide terminated poly(ethylene glycol)
PFA	Paraformaldehyde
pHEMA	Poly(2-hydroxyethyl methacrylate)
PPxY	proline-rich peptides
RGDS	Arginine-Glycine-Aspartic acid-Serine sequence
RNA	Ribonucleic acid
RT	Room temperature
SEC	Size exclusion chromatography
SH-ssDNA	Thiol-terminated ssDNA
S-S	Disulfide
ssDNA	Single stranded DNA
TBE	Tris/Borate/EDTA
TCEP	Tris-(2-Carboxyethyl) phosphine
T-SH	Thiol thymine
UC-MSC	Umbilical cord mesenchymal stem cell
v/v	Volume per volume
w/v	Weight per volume

Abstract

Injuries in the central nervous system (CNS) can lead to overwhelming consequences due to the inability of severed axons to regenerate beyond the lesion site. Patients that suffer from these injuries experience diverse sequalae's from reduced physical function to psychosocial limitations, among others. Currently, the treatment options do not constitute a cure. Transplantation of neural stem/progenitor cells (NSPC) offers the possibility of replacing lost neurons and supporting cells, leading usually to functional benefits in preclinical studies. However, the injection of NSPC as cell suspensions into the CNS shows poor cell survival and engraftment, as for limited differentiation along the neuronal lineage. Efforts to overcome these limitations, have been mainly focused on the development of biodegradable hydrogels, which besides providing structural support for cell anchorage and axonal regeneration, create a supportive niche for cell survival and differentiation.

In this work, we proposed to develop a novel fully-defined self-assembled hydrogel for application as co-adjuvant of NSPC-based transplantation therapies, based on DNA self-assembly. For that, a eight-arm maleimide terminated poly(ethyleneglycol) (PEG-MAL) was used as the polymeric backbone, Ac-GRGDSP*C*-NH_2 (RGDS) peptide as an instructive cue to promote cell adhesion and neurite extension of NSPC, and two complementary 20nt single stranded deoxyribonucleic acid (ssDNA) sequences to trigger self-assembly under physiological conditions. This approach would allow the combinatorial display of numerous bioactive cues and the independent tuning of the hydrogel mesh size and viscoelastic properties, by varying the DNA crosslinker concentration. The shear-thinning and self-healing properties of the DNA-crosslinked gels would ultimately allow the *in situ* delivery of NSPC through a small gauge needle into the injured CNS, therefore contributing to the survival of transplanted cells following transplantation.

To allow conjugation with PEG-MAL through SH-MAL addition reaction, the RGDS peptide with a cysteine and ssDNA with a 5' disulfide bond (C6 S-S) were used. While the conjugation of RGDS to PEG-MAL was straightforward that of ssDNA required the prior reduction of the C6 S-S-ssDNA disulfide bond to deprotect the thiol reactive group. Purified reduced SH-ssDNA sequences were successfully obtained after the optimization of the reducing agent (tris(2-carboxyethyl)phosphine (TCEP) and dithiothreitol (DTT)) and that of the purification columns. Still, the percentage of reactive thiols in SH-ssDNA was found to be dependent on the ssDNA sequence, varying from 45 to 76%.

Functionalization of PEG-MAL with pendent RGDS groups, was performed with different stoichometric balanced molar ratios of SH groups to PEG-MAL in order to functionalize 1 to 8 arms of the multi-arm PEG-MAL. In accordance to the literature, a high incorporation efficiency of RGDS was observed (as high as 95%), as determined quantifying the percentage of remaining free thiol groups in the reaction buffer.

Functionalization of PEG-MAL with SH-ssDNA was performed similarly, using different stoichometric balanced molar ratios of SH groups to PEG-MAL in order to functionalize 2, 4 and 6 arms of the multi-arm PEG-MAL. For a SH:PEG-MAL molar ratio of 4:1, the quantification of remaining free thiol groups in the reaction buffer revelead a high immobilization efficiency of ssDNA (≈ 97%). However, high-performance liquid chromatography (HPLC), gradient polyacrylamide gel electrophorese (PAGE) and size exclusion chromatography (SEC) showed the formation of polydisperse PEG-ssDNA ½ conjugates and suggested the establishment of dimers of SH-ssDNA during the 4-hour reaction with PEG-MAL.

Preliminary PEG-RGDS-DNA hydrogels were prepared, as proof of concept, with DTT-reduced, Microspin G25-purified ssDNA. Dynamic rheology revelead, for this hydrogel, a low storage modulus (≈ 17 Pa) suggesting a low degree of crosslinking. Despite its low stiffness, PEG-RGDS-DNA hydrogel, revealed a shear-thinning and self-healing behavior, as expected for a physically crosslinked hydrogel. By using gravity columns to purify DTT-reduced ssDNA, this issue is expected to be overcome.

In parallel, while PEG-RGDS-DNA hydrogels were ongoing optimization, we assessed the efficacy of the combined immobilization of HYD1 and AG73, two cell adhesive peptides with neurite-promoting ability, in enhancing neurite outgrowth of NSPC. For this purpose, fibrin (Fb) hydrogel was used as the platform for the 3D culture of NSC (H9-derived NSC) and functionalized gels prepared at input peptide concentrations previously optimized for individual peptides. We showed that peptide incorporation did not significantly impact either the storage or the loss moduli of fibrin gels. Moreover, qualitative assessment of H9-NSC behaviour revealed a tendency for a higher number of cellular sprouts protruding from the neurospheres in HYD1 and AG73-functionalized hydrogels, as compared to unmodified Fb gels. These promising results need now to be supported by additional image acquisition and quantitative image analysis, to assess if the combination of these peptides has an additive or even a synergistic effect on neurite outgrowth.

Overall, this thesis hopes to impact the development of engineered hydrogels for use as delivery vehicles of NSPC into injured CNS.

CHAPTER I

INTRODUCTION

Clinical Problem Addressed

1. Pathophysiology

Damage to the central nervous system (CNS) due to trauma, degeneration or genetic disorders can lead to permanent functional disability, due to the limited ability of CNS neurons to spontaneously regenerate and establish correct axonal connections [1]. CNS injury can be due to apoptotic and necrotic death of neurons, as well as astrocytes and olygodendrocytes. It can also be due to axonal injury, demyelination, ischemia, inflammation, lack of positive environmental stimuli, inhibition of axonal growth, among others [1–5] (Figure 1).

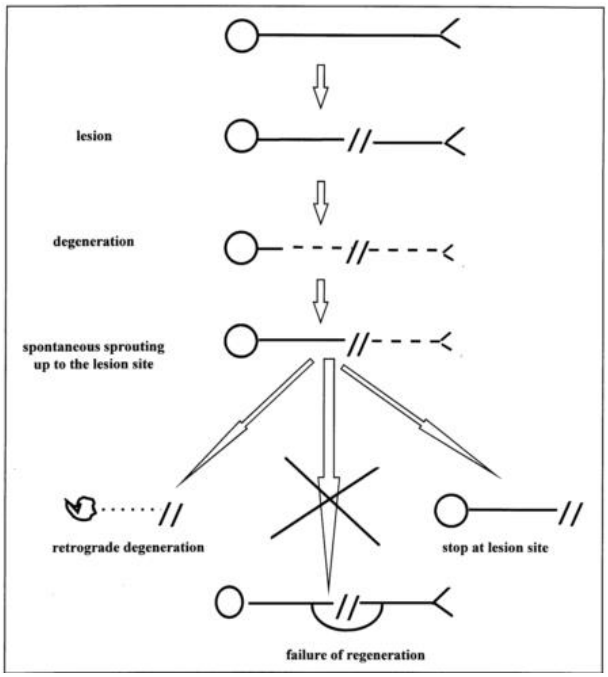

Figure 1. Pathological changes of lesioned axons in adult mammalian CNS. Scheme of lesion induced changes after axonal disruption in the adult mammalian CNS. Image reproduced from Stichel et al [5].

After CNS trauma, there is neuronal degeneration and cell death [4]. Damage of the CNS is usually characterized by reactive gliosis or glial scaring, where the cell cycle activation will play a major role in the activation and proliferation of astrocytes and microglia [2, 6].

After initial mechanical trauma, neural and vascular structures are disrupted, and immune cells infiltrate the lesion site [7–9]. The recruitment of inflammatory cells and reactive astrocytes over time leads to the formation of a glial scar, often accompanied

by a fluid-filled cyst [2, 7–9]. In parallel, the release of inhibitor molecules associated with myelin, fibrotic tissue or glial scar contribute to the failure of axonal regrowth through a physical and biomechanical barrier to neural outgrowth [2, 7].

Nevertheless, infections in affected patients impede neurological recovery as well as increased morbidity and mortality. These secondary effects can be related to exposure of these patients to invasive medical procedures, hospitalization, among others, since damaged CNS downregulates the immune system [8]. These infections in the CNS usually translate into pneumonia, and are usually associated with strokes, traumatic brain injury and spinal cord injury [8].

2. Epidemiology and Economic Impact

According to the World Health Organization (2006) [10], patients that suffer from neurological disorders can present diverse sequalae's, including physical functional limitations, cognitive impairments, behavioral problems, communication impairments, affected basic living activities as well as psychosocial limitations. By evaluating traumatic brain injury in 2012, 1.5 million Americans sustain that injury anually and 5.3 million live with permanent disability due to this [11]. Since the effects are severe and incurable, $56.3 billion is spent, annually, on direct and indirect costs of traumatic brain injuries [11].

Neurological disorders constitute 12% of total deaths globally [10, 12]. These numbers are related to the long-term effects persistent throughout life as well as the severe disability and handicap of the patients [1, 13, 14].

However, since it is necessary to consider the development of new treatments for brain diseases, it is also really expensive to design. The costs of development, discovery, and phase I clinical trials can go up to US$100 million, and around US$1 billion before reaching the customer [15].

3. Current Treatments

Currently, in clinics, there are some treatments used in injured CNS, like the delivery of anti-inflammatory drug Methylprednisolone and surgical decompression in order to relieve pressure generated by progressive edema and hemorrhage, in order to protect the neural elements that initially survived the injury [16, 17].

However, these are not effective treatments since all the therapies are focused on either regeneration of axons, and the remission or replacement of dead neurons.

Nevertheless, they will always have to pass through the glial scar environment mentioned earlier [6, 13]. Not only that, but the majority of the currently available treatments are symptomatic and aim to halt or ameliorate damage [15].

Cell Therapies

With the advances in the field of stem cell biology and regenerative medicine, cell therapies gave a new hope to patients with CNS injuries, via the delivery of different cell types (Figure 2) [18]. A multitude of cells have been explored for transplantation into the damaged CNS, including: i) embryonic stem cells (ESCs) or induced pluripotent stem cells (iPSC) differentiated towards the neural lineage, including neural stem cells (NSC), committed neural progenitors such as oligodendrocyte progenitor cells and neuronal-restricted progenitors, as well as differentiated neuronal cell types such as motor and dopaminergic neurons; ii) NSC isolated from human fetal CNS tissue; iii) NSC directly converted from adult somatic cells (iNSC); iv) mesenchymal stem cells derived from the umbilical cord or the bone marrow; v) olfactory ensheathing cells; and vi) differentiated cell types [19]. Cell transplantation is usually associated to functional benefits in pre-clinical trials, either by directly integrating into the tissue or indirectly by secreting factors [13]. However, transplanted stem cells have to be engineered for functional advantage, otherwise, they will not contribute to long term recovery of the damaged CNS [21].

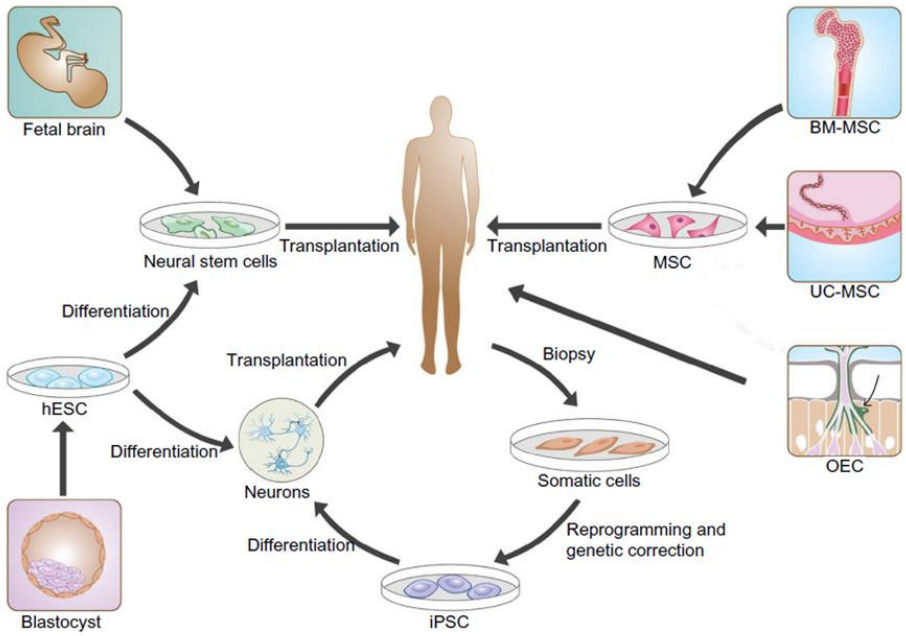

Figure 2. Cell sources for transplantation into the injured CNS : hESC (human embryonic stem cells) isolated from the inner cell mass of a blastocyst; neural stem cells from fetal brain or spinal cord; BM-MSC (bone marrow-derived mesenchymal stem cells) isolated from adult bone-marrow; UC-MSC (umbilical cord mesenchymal stem cells) from umbilical cord of newborns; OEC (olfactory ensheathing cells) from adults or fetal olfactory bulb tissue; and iPSC (induced

pluripotent stem cells) derived from reprogrammed somatic cells. Image adapted from Han et al.(2014) [18]

Drug therapies to treat this type of CNS damage can be by directly stimulating growth (neurotrophic), by saving spared neurons from degeneration (neuroprotective) or even by alleviating the toxic environment around the injured site (neutralizing) [20].

The neuroprotective approaches recently concluded or ongoing clinical trials are the sodium channel blockade, delivery of the anti-inflammatory drug minocycline, delivery of granulocyte colony stimulating factor and basic fibroblastic growth factor (bFGF) [21–23]. On the other hand, the neuroregenerative approaches are based on cell therapies, delivery of chondroitinase ABC, antagonism of neurite outgrowth inhibitors (as NOGO-A, already in clinical trials), use of bridging support matrices and intermittent exposure to hypoxia [24–26]. The electrical stimulation of spared neurons is, also, already in use to treat this condition in order to enhance plasticity [27].

In 2005, following the work of Steve Goldman, there was an increasing interest in the use of multipotent neural stem cells, due to their ability of giving rise to both neurons and glia and act as substrates for repair of the brain and the spinal cord [28].

Although, before starting any therapy for neurological injuries there are four issues that should be considered: i) if the cell-based approach is clinically competitive and what risks for the patient are acceptable; ii) the disease pathology should determine which cells should be generated from the stem cells; iii) it should be demonstrated in animal models that the stem-based treatment induces substantial improvement of functional deficits, and iv) it is necessary to precisely determine the biological mechanisms underlying the stem cell treatments [29].

Some treatment options can include transplantation of a multitude of cells, such as neural stem/progenitor cells (NSPC), iPSC and their differentiated progeny, among others into the injured/diseased CNS [1, 30, 31].

1. Neural Stem Cells

Currently, the most promising cells for physiologic repair of CNS lesions, functional recovery and neuropathic relief are NSPC thanks to their ability to secrete cytokines with neurotrophic and immunomodulatory effect, as well as considering their contribution to the remyelinization of spared axons and establishment of relay neural circuitries [28, 30,

32]. They can proliferate in an undifferentiated state *in vitro*, which allows them to expand mitotically and harvested in bulk for future use [33]. They are undifferentiated cells that

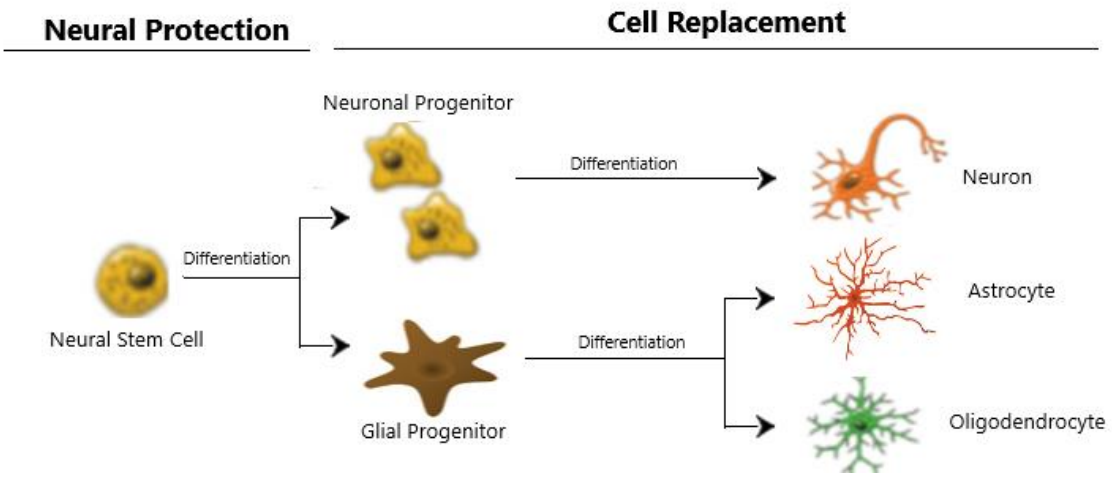

are able to both self-renew and generate the three major cell components of the CNS: neurons, astrocytes and oligodendrocytes (Figure 3) [33–38].

Figure 3. Therapeutic potential of NSC. The transplantation of NSC aims to regenerate the damaged CNS, through the reestablishment of the neuronal circuitry as well as restoration of the neurological functions. Image based on the work from Tang et al. and IGP Group from Uppsala Universitet [38, 39]

Previous studies from Lu *et al* (2012), Lindvall and Kokaia (2010), Okano (2010) and, more recently Lu *et al* (2017), showed that transplanted NSPC and human ES-derived NSPC were capable of dividing, differentiating and integrating into the injured tissue, with formation of relay neuronal circuitries, leading to approval of clinical trials to assess the safety and preliminary efficacy of human fetal CNS-derived NSC transplantation [3, 29, 33, 40, 41]. According to Lu *et al* (2017), on a period of 18 months, the NSC implanted continued stem cell maturation, indicating that maturation is retained by NSC placed in sites of neurotrauma [41]. They also report improvements in function after mature cell markers of both neuronal and glial lineages are expressed [41]. Jeong *et al* (2003) and Zhu *et al* (2011) also demonstrated that the transplantation of NSC into injured CNS can improve functional outcome, since they can differentiate into mature neurons [42, 43].

The implanted cells will have a neuroprotective role and can reduce pro-inflammatory cytokines, reactive oxygen species, and astrogliosis, as well as enhance host neural stem cell to oligodendrocytes differentiation and stimulate remyelination, in addition to leading to improved axonal conduction [29, 32, 35].

Taking into account previous works, the ideal timeline window for transplantation of NSPC is between 9 to 15 days following injury, after the acute inflammation phase and before the astroglial scar becomes prominent, even so, only a small number of cells is originated [32, 33, 44].

ESCs have a higher proliferative capacity and efficiency regarding neuronal differentiation when compared with somatic NSPC [30], and their transplantation was already approved in clinical trials for the reason that they were able to survive, divide, differentiate and promote functional recovery in rodent models [45–49].

2. Current Limitations

When it comes to the transplantation of cells directly to the injury site, numerous studies show that fewer than 5% of injected cells persist at the site of injection within days of transplantation. Concerning the work of Parr *et al* (2008), after 7 days of transplantation, 4.6% of the NSPC survived, but after cell phenotyping, it was demonstrated that 18.6% were astrocytes, 63.4% oligodendrocytes and only 1.1% were neurons [44].

In order to address these problems, it is important to establish two main approaches regarding the type and main focus of the treatment: i) the delivery of new cells and promotion of their ability to integrate completely with the host tissue, and ii) to promote endogenous cell stimulation and regeneration by the delivery of drugs or protein therapeutics [20]. When it comes to the means of delivery the treatment, it is best to aim in biomaterials to perform the passage through the blood-brain barrier (BBB), such as hydrogels or even nanoparticles [1, 36, 50]. For a typical cell-therapy procedure, it is important to: i) prepare the cell suspension in vitro; ii) have designed the injection procedure; iii) measure the retention of the administered cells post-injection [51]. However, there is not a standardized administration protocol, for efficient injectable cell transplantation that can accurately characterize cellular health post-injection (Figure 4) [51].

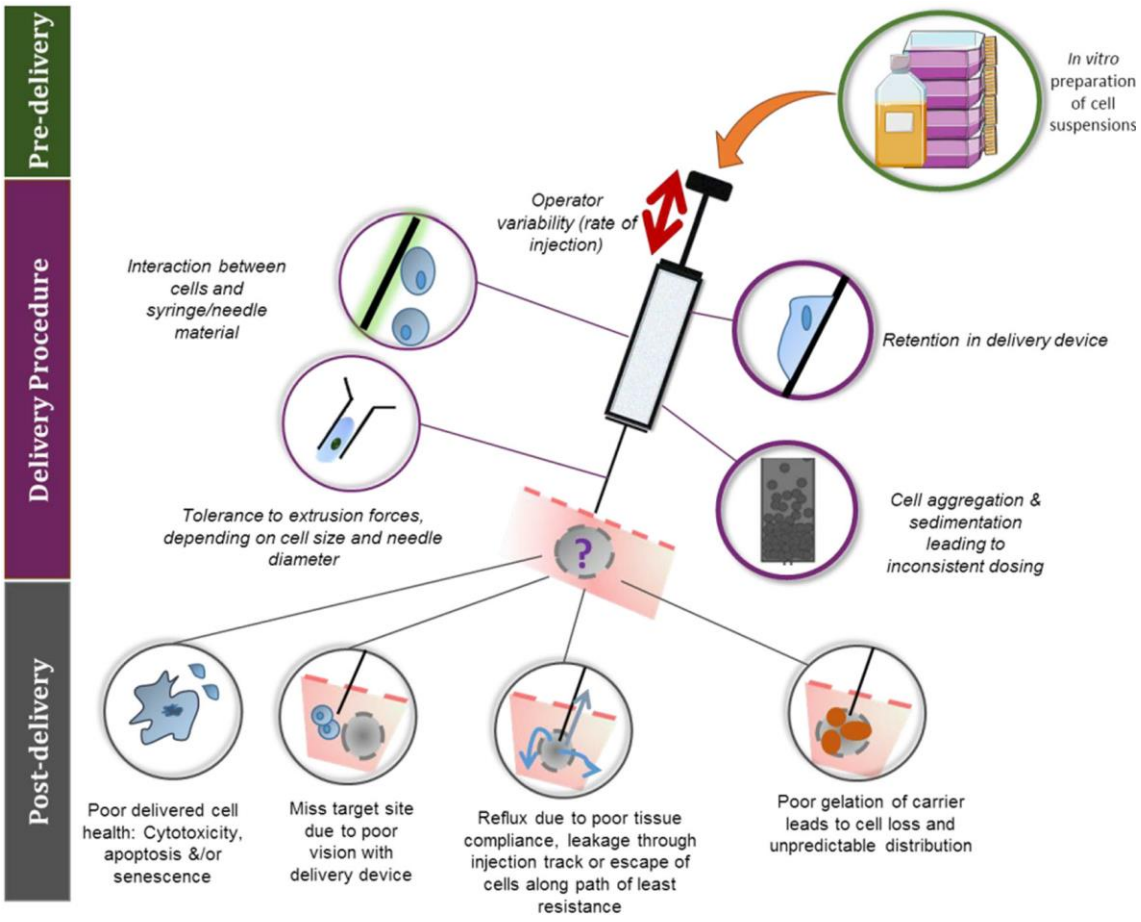

Figure 4. Common problems using injectable delivery of cells and their possible fates. A cell-therapy protocol has three stages: in vitro preparation (pre-delivery), injection (delivery) and subsequent retention (post-delivery). Image reproduced with permission from Amer et al. [51].

Hydrogels as vehicles for NSPC transplantation

Biomaterials are gaining increasing relevance in the field of bioengineering, especially because they can be used for a wide range of therapies. They can be used to deliver therapeutic molecules, such as growth factors, proteins, small molecules and even the cells specified before as well as being applied as space-filling agents and three-dimensional structures that organize and present stimuli for cells and for the formation of the desired tissue [13, 20].

Hydrogels are three-dimensional (3D) water-swollen polymeric networks (over 90% of water) comprised by crosslinked hydrophilic polymers which are particularly compelling for application in soft tissues, such as the CNS [13, 20, 44, 45]. They can be used as space-filling agent specifically designed to provide the necessary stimuli to direct the infiltration of endogenous cells, or to act as 3D temporary support matrices to assist cell transplantation and promote tissue remodeling and regeneration tissue [20, 48]. They also exhibit high permeability to oxygen, nutrients and other water-soluble metabolites [55]. To allow host or graft cell infiltration they can be engineered to present biodegradability or dissolution via enzymatic, hydrolytic, or environmental pathways [53], [54], [56], [57].

Additionally, hydrogels can conform to the shape of the surface to which they are applied and be in many different physical forms such as solid molded forms, pressed powder matrices, microparticles, coatings, membranes or sheets, encapsulated solids along with liquids [52, 53].

1. Hydrogels Backbone

Hydrogels can be made from essentially any water-soluble polymer, including a wide range of chemical compositions and with a bulk of physical properties [53]. Depending on their composition, hydrogels may be prepared from either synthetic or natural polymers.

1.1. Naturally Derived Materials

Hydrogels based on naturally derived biomaterials have been historically favored for the development of injectable hydrogels for cell delivery into the CNS, due to their inherent bioactivity and mechanical properties similar to those of the natural extracellular matrix (ECM) [31]. The polymers that have been most explored for this purpose include

fibrin gel, hyaluronic acid (HA), collagen, laminin/collagen mixtures, laminin-functionalized agarose, and alginate [20, 31, 51, 58, 59].

Fibrin (Fb) is a Food and Drug Administration (FDA) approved hydrogel with widespread clinical use as a haemostatic agent, in skin substitutes, as well as in drug delivery systems [20, 59]. Fibrin is a natural polymer formed during the blood coagulation cascade from its zymogen form, fibrinogen, with a central role in haemostasis. Owing to its, inherent biocompatibility, tunable mechanical properties, susceptibility to proteolytic degradation, and ability to be injected and polymerize *in situ*, Fb has been successfully explored for the transplantation of NSPC [3, 41]. A schematic view of fibrinogen structure and of fibrin polymerization can be seen in Figure 5 and 6 [61].

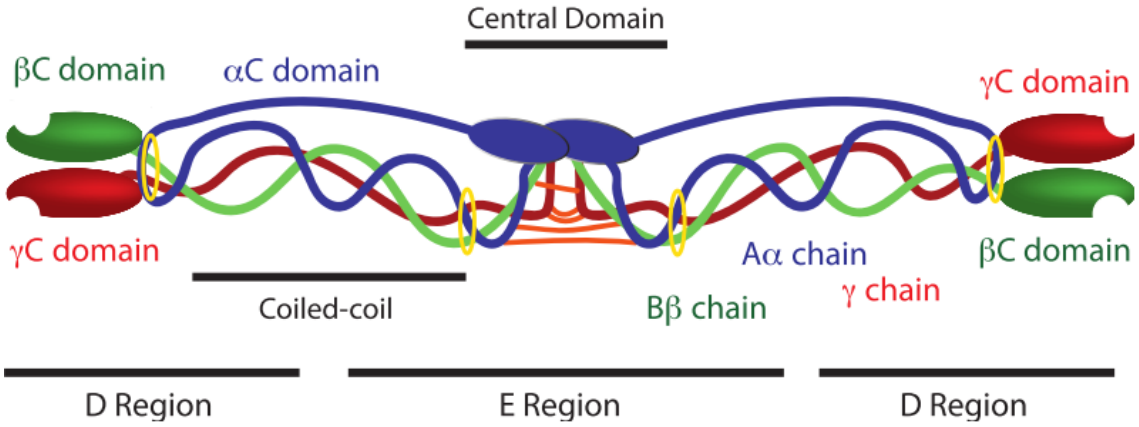

Figure 5. Fibrinogen structure. It is composed by three distinct chains (Aα, Bβ and γ). The interchain disulfide bridges (orange) connect the six polypeptide chains in the central domain, and disulfide rings (yellow) stabilize the coiled-coil regions. Image reproduced from Brown and Barker (2013) [75].

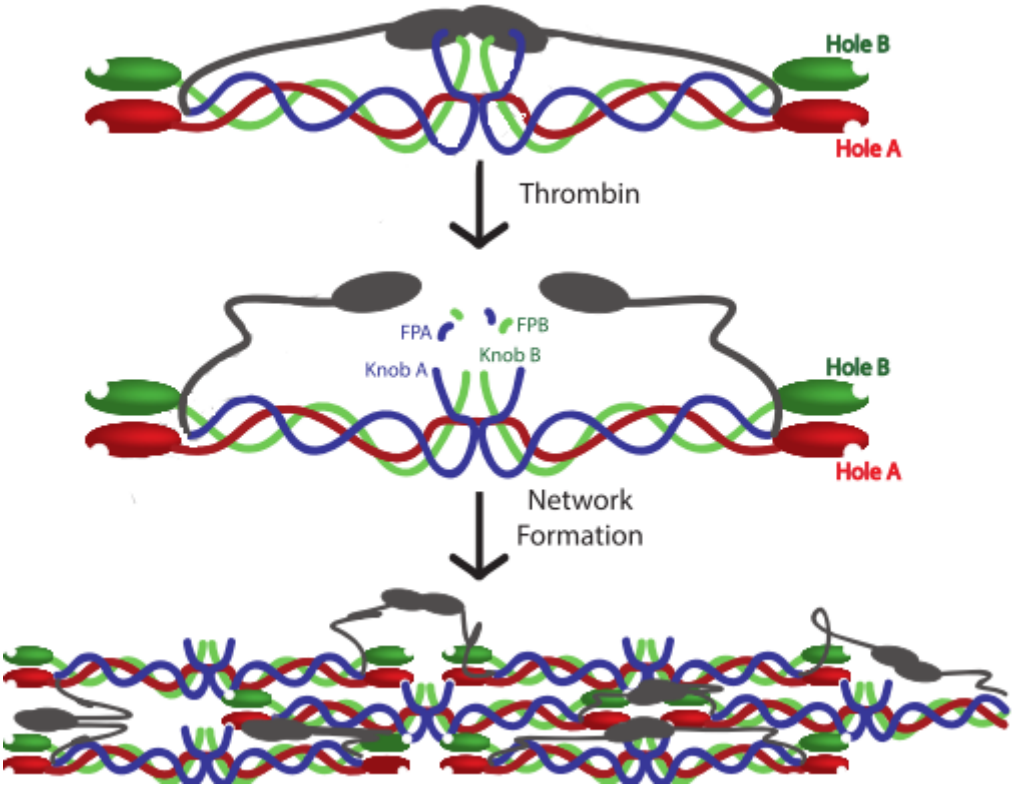

Figure 6. Fibrin Polymerization. α chains - blue; β chains - green; γ chains - red; αC domains – gray. After conversion of fibrinogen into fibrin, fibrinogen αC-domains containing the RGD recognition motif form ordered αC polymers. FPA, fibrinogen peptide A. FPB, fibrinogen peptide B. Image reproduced from Brown and Barker (2013) [75].

1.2. Synthetic Materials

Synthetically based hydrogels based on synthetic polymers have advantages as compared to hydrogels based on naturally-derived polymers. Synthetic hydrogels are attractive to this field because of their composition, molar mass, and properties since they are reproducible and controllable. These hydrogels present a lower risk of immunogenicity and higher versatility, namely by allowing a more precise control of the hydrogel bulk properties, bioactivity and degradation [20], [31], [62][20], [31], [62][20, 31, 62]. In this sense, it is possible to reproducibly produce synthetic polymers with specific molecular weights, block structures, degradable linkages as well as crosslinking modes, and it is possible to include reactive functional groups for crosslinking and for subsequent biofunctionalization [20, 31]. All these properties will determine the gel characteristics, such as gel formation dynamics, crosslinking density and the material mechanical and degradation properties [31].

The most explored synthetic polymers for the development of cell carriers are peptide-based synthetic hydrogels and poly(ethylene glycol) (PEG) hydrogels [11, 58, 63].

Peptide-based synthetic hydrogels are based on engineered proteins, which, due to its synthetic nature can also be included as a synthetic hydrogel, since precise control over the primary sequence and molecular weight can be achieved. Allowing the fine-tuning of the gelation process as well for its structural and mechanical properties [63].

PEG is an extremely versatile hydrophilic and biocompatible polymer widely used in clinic [64], with advantageous properties for application as cell carrier in cell-based therapies [60, 65, 66]. Although PEG lacks bioactive domains, it can be synthesized to include reactive functional groups to provide suitable sites for the chemical binding of cell instructive physical cues, such as cell adhesive domains and proteases-sensitive sequences [63, 65]. Moreover, the physical properties of PEG-based hydrogels may be easily tailored by varying the molecular weight of PEG chains, as well as crosslinking degree, which allows the design of hydrogels with tunable stiffness, and structure [11, 31, 67].

There are important differences when it comes to linear and star PEG, being that multi-arm star shaped PEG can easily induce the formation of stereo-complexes, a relevant feature in biomedically hydrogel systems, as well as faster formation, greater degree of modification and superior in three-dimensional culture when comparing 4-arm PEG to 8-arm PEG [66, 68]. 8-arm star PEG also allows for a more precise control of the mechanical properties of the hydrogel, resulting in a larger spectrum of tissue engineering applications [66]. The most common approach to obtain PEG-based hydrogels is through photopolymerization, which use ultraviolet (UV) radiation to induce the crosslinking of acrylated PEG molecules with the formation of a 3D hydrogel. More recently, protease sensitive peptides flanked by two cysteines residues have been explored for crosslinking of PEG. These react with unsaturated groups of end-functionalized multi-arm PEG leading to hydrogel formation [65]. It is also possible to attach pendent cell adhesive ligands to star-PEG to promote neurite outgrowth, but this modification leaves fewer “free” reactive arms available for crosslinking (Figure 7) [11, 66].

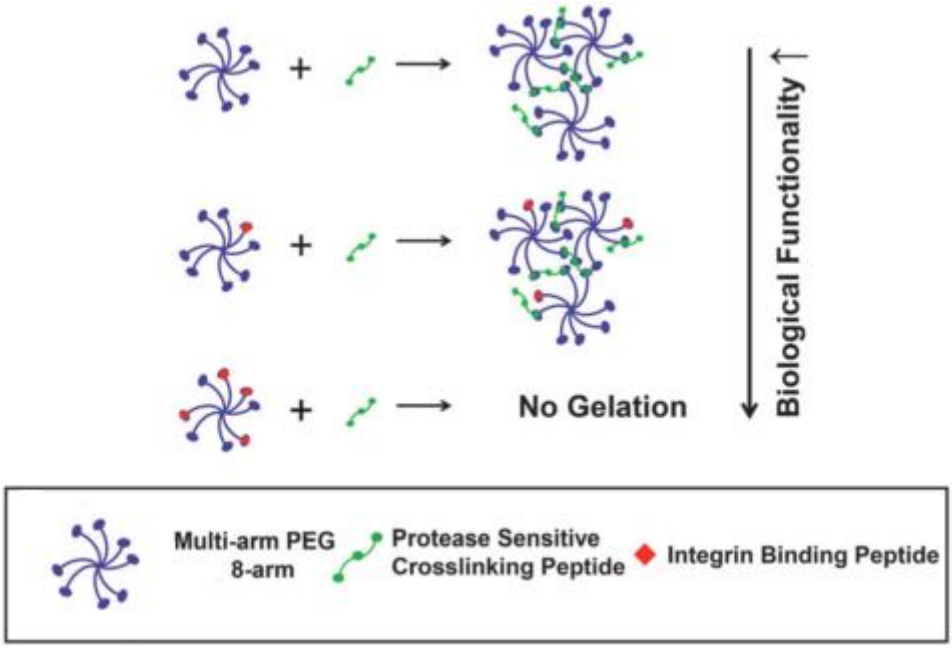

Figure 7. Crosslinking mechanism for peptide modified 8-arm PEG and crosslinking peptides, through Michael-type addition. Bioactive modification with integrin binding peptides affects crosslinking kinetics by binding with the reactive sites of PEG, preventing network growth at those sites. Image from Kim et al (2016) [66].

Owing to its low immunogenicity, covalently-crosslinked PEG hydrogels have been successfully explored for cell and drug delivery into the CNS [69] as well as a three-dimensional platforms for NSPC expansion and differentiation [70].

2. Type of Crosslinking

When designing a hydrogel there is a need for a crosslinking agent. The crosslinkers can be chemical or physical, presenting distinctive characteristics depending on how the network is made. Their highly porous structure can be simply tuned by controlling the density of crosslinkers in the matrix and the affinity of the hydrogels for the aqueous environment in which they are swollen [53].

In order to assure the viability of living cells inside the gels, it is important that the resultant porosity allows the diffusion of small molecules, such as nutrients, gases, and metabolites, while also maintaining the same characteristics over time (Figure 8) [54, 64].

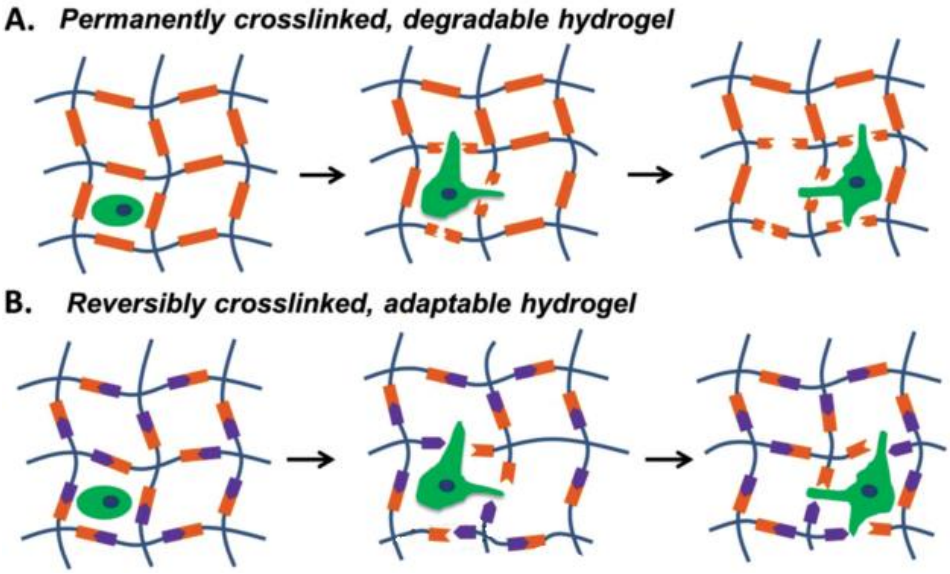

Figure 8. Type of Crosslinking. A) Schematic of permanently crosslinked hydrogels which irreversible degradation required to allow cell migration eventually leads to hydrogel bulk degradation. B) Schematic of an adaptable hydrogel witch, due to their shear-thinning and self-healing properties, allow cell migration through breaking and re-formation of the reversible linkages and, as a result, the maintenance of its long-term integrity. Image from Wang and Heilshron [64]

2.1. Chemical Crosslinked Hydrogels

This type of hydrogels relies on chemical reactions where covalent bonds are established to bind the polymeric chains of the hydrogel backbone [52, 54, 57]. They have the advantage of preventing both the dissolution of the hydrogel matrix and its diffusion away from the site of injection [53]. Chemical crosslinking has been explored to form *in situ* polymerizing hydrogels. However, to allow injectability, the reactive gel precursor solutions have to be kept separate prior to injection or alternatively, the polymerizing solution needs to be injected just before the gelation time. At a constant polymer concentration, by varying the crosslinking degree the mechanical strength, stability and swelling properties of the hydrogel can be tuned [71].

Also, chemically-crosslinked hydrogels are not homogeneous since they contain “clusters”, which are regions of low water swelling and high crosslinking density, that are dispersed in regions with the opposite features [52]. Furthermore, these hydrogels can

have free chains ends that represent gel network “defects” and do not contribute to the elasticity of the network [52].

Many chemistries have been explored for *in situ* crosslinking hydrogels. The crosslinking groups can be added to reactive pre-polymers as small molecules or conjugated directly to them. Examples of covalently-crosslinked hydrogels are hydrogels formed through hydrazine bonds *via* reaction of an aldehyde and a hydrazide as well as those formed through Michael-type addition between a nucleophile and a vinyl-sulfone or maleimide group, which promotes rapid crosslinking of the network [53, 57]. Michael-type addition reaction also allows the functionalization of inert hydrogels with cell adhesive moieties, followed by crosslinking with protease sensitive peptides [66].

2.2. Physically Crosslinked Hydrogels

Physically-crosslinked hydrogels can be achieved using a variety of environmental triggers as well as a variety of physicochemical interactions while avoiding the use of crosslinker agents [52, 53, 56, 57, 63]. They are also not homogeneous, due to the clusters of molecular entanglements, or hydrophobically- or ionically-associated domains, which can create inhomogeneities, and have lower gelation time. Still, physically-crosslinked hydrogels owing to their shear-thinning (viscous flow under shear stress) and self-healing properties (time dependent recovery upon relaxation) are injectable, and do not, necessarily, need the matrix to degrade in order to allow cell spreading and cellular infiltration [52, 72].

On the other hand, one limitation of these hydrogels is the difficulty in achieving robust mechanical properties, since a large amount of polymer is necessary to increase mechanical stiffness [72]. However, neural stem cells are responsive to mechanical stimuli and softer substrates (storage moduli in the range of 0.1 to 1 kilopascal), being more permissive to neuronal differentiation [63]. Due to that, the type of crosslinking used for these hydrogels needs to be carefully thought.

2.2.1. Hydrophobic Interactions

With this approach, polymers with hydrophobic domains are able to crosslink in aqueous environments via “sol-gel” chemistry, also known as reverse thermal gelation [53, 56, 57]. The main driving force for this assembly is the net entropic increase that results from burying the hydrophobic faces away from the bulk aqueous environment, which releases surface-bound water molecules when two or more hydrophobic surfaces assemble. These type of self-assembly can organize structures such as hydrogels and polymeric micelles that can be used for cell encapsulation [54, 56, 57].These types of interactions are used in self-assembly of block copolymers to form a variety of phases

and are excellent candidates for the assembly of adaptable hydrogel networks. Can also be used to form hydrogels comprising polypeptides and a synthetic polymer such as PEG [54].

2.2.2. Biorecognition-interactions

The concept of protein-protein interaction between specific association domains was explored by Heilshorn's group for the design of mixing-induced two-component hydrogels (MITCHs) [73, 74]. The first component of such system comprises proline-rich peptides (PPxY) linked by hydrophilic spacers [73, 74]. The second is composed by engineered repeats of WW domain linked together by hydrophilic spacers containing the cell adhesion motif RGDs [73, 74]. MITCHs were successfully investigated for cell encapsulation and growth-factor delivery. Hydrophobic interactions and supramolecular chemistry can be used to facilitate the formation of denser and/or more stable networks in self-assembled systems [53]. Their properties can alter by changing the network topology as well as crosslinking point density [75].

Neural stem cells encapsulated within these hydrogels form stable three-dimensional cultures with neurite differentiation and outgrowth, as well as spreading [74], [76].

2.2.3. Electrostatic Interactions

This type of crosslinking is the most investigated when it comes to *in situ* gelling polymers due to the fact that their polymerization can be done at physiological pH and at room temperature [53, 57]. The main advantage is that biodegradation can happen while ionic species in the extracellular fluid bind to the hydrogel components, breaking down the network [53]. Alginate hydrogels formed through crosslinking by divalent ions (usually calcium) is a common example of hydrogels formed via electrostatic interactions.

2.2.4. Hydrogen Bonding Interactions

These interactions can be used to produce hydrogels *in vitro* by freeze-thawing and can also be used to formulate injectable hydrogels [53]. The viscoelastic properties of the polymer blends are more gel-like than those from the constituent polymers measured independently [53].

2.2.5. Peptide Conformation

Peptides can be designed to form secondary structures (nanofibers) through the establishment of hydrophobic, ionic or hydrogen bonding interactions, leading to the formation of a self-assembled hydrogel. This type of gels can be engineered to exhibit epitopes to induce the proliferation and function of specific cell types, including of neural stem cells, however, their mechanical properties cannot be modulated [71].

In the case of CNS, they allow neuronal attachment, neurite outgrowth and synapse formation [71].

2.2.6. Stereocomplexation

Stereocomplexation refers to synergistic interactions that can occur between polymer chains or small molecules of the same chemical composition but different stereochemistry [53].

This crosslinking method can also help form more robust, in situ hydrogels with high storage module by taking advantage of the interactions between polylactide blocks with L- and D- stereochemistry [53, 57, 71].

2.2.7. Deoxyribonucleic Acid (DNA) Interactions

An unprecedent development of DNA nanotechnology made it possible to form hydrogels in situ involving the use of specific molecular recognition motifs [53].

Despite the high costs associated with DNA synthesis, DNA has several advantageous features as a physical crosslinker for formation of self-assembled hydrogels [63]. These include its hydrophilic nature, ability to form stable and flexible secondary structures through specific Watson-Crick base-pairing and inherent biocompatibility (Figure 9) [54], [56], [63], [77].

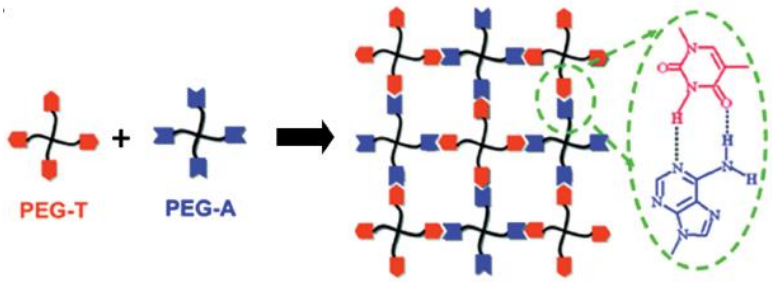

Figure 9. Schematic of hydrogel self-assembly via intermolecular, hydrogen bonding of Watson-Crick base pairs. Image from Wang et al (2012) [57]

One of the advantages of using DNA as a crosslinking agent is that it can be easily tailored by varying the number and type of nucleic bases or through the incorporation of bioactive motifs [63, 77, 78]. As a result, the properties of DNA crosslinked hydrogels can be easily tuned by altering DNA length, concentration or even the structure. Also, it is possible to alter the storage modulus from several Pascal to several thousand Pa, while maintaining their thixotropic ability without altering their topological network [75, 77, 79–81]. According to Li *et al* (2016), the mechanical properties of DNA-crosslinked

hydrogels is dictated by the stability of the crosslinker, meaning that the storage modulus (G') of a hydrogel formed via DNA crosslinking can vary without altering the crosslinking density and the structure of the hydrogel network [75]. Finally, due to the well-known melting point of the DNA, DNA crosslinked hydrogels are thermoreversible [80]. Therefore, by realizing many changes there can be various physical, chemical and biological stimuli employed together, translating into an augmented flexibility in designs [81].

Still, this approach is far from being a treatment translated into clinic. However, the only studies already performed for this type of crosslinked hydrogels are regarding their mechanical properties (between 63 and 600 Pa) [68], their macroscale integrity and response to reducing conditions via disulfide bond cleavage [82], direction of stem cell differentiation [81]. The most interesting study in this area is from Jiang *et al* (2010), who design a DNA crosslinked polyacrylamide hydrogel with cultured rat embryonic spinal cord cells *in vitro* to study neurite outgrowth, presenting an increase of axonal length [83]. However, the cell studies were performed on top of the hydrogels, not indicating the cells migration. For that, Wang *et al* (2017) made pure DNA hydrogels with HeLa cells, and reported a downward and laterally migration of the cells, *in vitro* [84]. These results indicate that, although physically crosslinked, these type of hydrogels present valuable characteristics when considering the transplantation of NSC.

3. General Requirements of Hydrogels for Cell Delivery into the CNS

Ideally, hydrogels for NSPC transplantation should be biocompatible and biodegradable on cell demand to allow neurite outgrowth and cellular infiltration, whilst providing a physical scaffold to retain the cells at the injection site [1, 80]. The native extracellular matrix of the CNS includes proteins, proteoglycans, as well as glycosaminoglycans which are recognized by cell surface receptors, triggering cellular processes. As such, hydrogels for NSPC transplantation should be able to mimic the biological and the physical properties of the natural extracellular matrix of CNS tissue, to control the fate of transplanted cells, namely in terms of cell survival, proliferation, migration, and neurite extension. The incorporation of short cell adhesive peptides with neurite-promoting ability, capable to emulate certain of the biological properties of full-length ECM proteins, has been explored for this purpose [85]. Comparing to the native ECM proteins, short adhesive peptides are less immunogenic while allowing the immobilization of a higher density of bioactive epitopes. [86, 87]. In Table 1 a list of cell

adhesive sequences explored to engineer hydrogel matrices for application in the CNS is provided. This includes the synthetic peptides HYD1 and AG73 recognized by α6β1 integrin and syndecan receptors, respectively, which were recently explored by our group to enhance the bioactivity of fibrin hydrogels towards ES-derived NSPC [88].

Table 1. Cell adhesive sequences explored to engineer hydrogel matrices for application in the CNS, and correspondent biological effect [89]

Sequence	***Derived from***	***Biological effect***
IKVAV	Mouse LN α1 chain	Neurite outgrowth, neuronal differentiation of NPC, migration, NSPC survival
Cyclic IKVAV	Mouse LN α1 chain	hNSC adhesion, migration and neuronal differentiation
YIGSR	Mouse LN α1 chain	Neurite outgrowth, extension and NPC survival
RNIAEIIKDI	Mouse LN γ1 chain	Neurite outgrowth (DRGs) [90]
PPFLMLLKGSTR (G3P)	LG3 module of LN 332 α chain	NSC adhesion and survival [91]
RKRLQVQLSIRT (AG73)	LG4 module of mouse LN α1 chain	Neurite outgrowth (PC12 neuronal cells) [92, 93] H9-derived NSC cell outgrowth [89]
RGD	Fibronectin, LN*, collagen and fibrinogen	Neurite outgrowth (DRGs) [90]
RGDS	Fibronectin	Neurite outgrowth, extension, hES-NPC adhesion and neuronal differentiation [94]
CGGNGEPRGDTYRAY [bsp-RGD(15)]	Rat bone sialoprotein	NSC adhesion [95]
DGEA	Collagen type I	Neurite outgrowth (DRGs) [96]

Other natural-derived cell adhesive ligands		
Sequence	***Derived from***	***Biological effect***
HAV	EC1 domain of N-cadherin	Neurite outgrowth (DRGs) [90]
HAVDIGGGC (HAVDI)		hiPS-NSC survival and neural differentiation [97]
Non-natural cell adhesive ligands		
Sequence	***Derived from***	***Biological effect***
SKPPGTSS (BMHP1)	Phage display peptide library	NSC adhesion and neurite outgrowth [98], [99]
PFSSTKT (BMHP2)		
KIKMVISWKG (HYD1)	Ligand for α6β1 integrin (identified from random peptide display library)	Cell outgrowth of mES-NSPC and H9-derived NSC [88], [89] Neurite extension (DRGs) [88]

Neural stem cells are responsive to mechanical stimuli and softer substrates with storage moduli in the range of that of human brain tissue (0.1-1 kilopascal (kPa)) are more permissive to neuronal differentiation [37, 66, 78]. In fact, by modulating the mechanical properties of the hydrogel, it is possible to better understand the conditions behind the promotion of neurite elongation, branching, and axonal regeneration as well as the possibility to differentially controlling neuronal and astroglial populations [66]. As a result, hydrogels with tunable physical properties are desirable when envisaging NSPC transplantation, to allow precise control over stiffness, structure, porosity, and permeability. Much desirable are also hydrogels with adaptable hydrogel networks, to permit cell migration while maintaining their long-term integrity and strength [1, 100]. Finally, a crucial issue for their clinical use is to be able to be precisely injected into the CNS through the use of minimally invasive procedures, to preserve the remaining healthy neural tissue. In fact, multiple studies report the advantages of the use of injectable hydrogels comparatively to other delivery methods, namely from Guvendiren *et al* (2012), D. Lu *et al* (2012) and Gaffey *et al* (2015), [101–103]. Injectability relies on the ability of the hydrogel to pass, as a liquid, through a small gauge needle and withstand a rapid sol-gel transition at the desired site [101]. This allow the hydrogel to take the shape of

the cavity, present a good fit and a good interface between the hydrogel and the damaged tissue [101]. Physically crosslinked hydrogels are ideal candidates for this purpose, due to the noncovalent nature of the crosslinks. Their shear thinning properties (viscous flow under shear stress) enable syringe needle injection of cell-carrying hydrogels already in the gel phase, which, besides protecting cells from the mechanical forces experienced during flow, can prevent cell dissemination into off-target sites of the CNS [102].

Aim of the Project

The aim of this work was to develop a novel fully-defined self-assembled hydrogel for application as co-adjuvant of NSPC-based transplantation therapies. This was engineered to present stiffness comparable to that of the CNS and to support the self-renewal and neuronal differentiation of NSPC.

For this purpose, a multi-arm poly(ethylene glycol) maleimide (PEG-MAL) was used as polymeric backbone, pendent neurite-growth-permissive adhesion ligands as cell-instructive cues, and deoxyribonucleic acid (DNA) hybridization to trigger self-assembling under physiologic conditions. This approach would allow the combinatorial display of multiple bioactive cues and the independent tuning of the hydrogel mesh size and viscoelastic properties, by varying the DNA crosslinker concentration.

The shear-thinning and self-healing properties of the DNA-crosslinked gels would ultimately allow the *in situ* delivery of NSPC through a small gauge needle into the injured CNS, therefore contributing to the survival of transplanted cells following transplantation. Finally, the bioactivity of the gel together with the dynamic nature of gels's non-covalent crosslinking bonds would be expected to positively impact the fate of transplanted cells, namely in terms of cell migration, neurite extension and integration into the host tissue, and the overall efficacy of NSPC-based therapies.

In parallel, the efficacy of the combined incorporation of the neurite-growth-promoting adhesive peptides HYD1 and AG73 (recognized by α6β1 integrin and syndecan receptors, respectively) in promoting neurite outgrowth of NSPC was assessed. As PEG-RGDS-DNA hydrogels were still ongoing optimization, these studies were performed using fibrin hydrogel as the platform for the 3D culture of NSPC. Due to the modulatory role of syndecans on integrin signalling the combination of AG73 with HYD1 was expected to synergistically increase NSPC cell outgrowth.

CHAPTER II

MATERIALS AND METHODS

1. Schematic view of the proposed approach for the preparation of PEG-DNA hydrogel

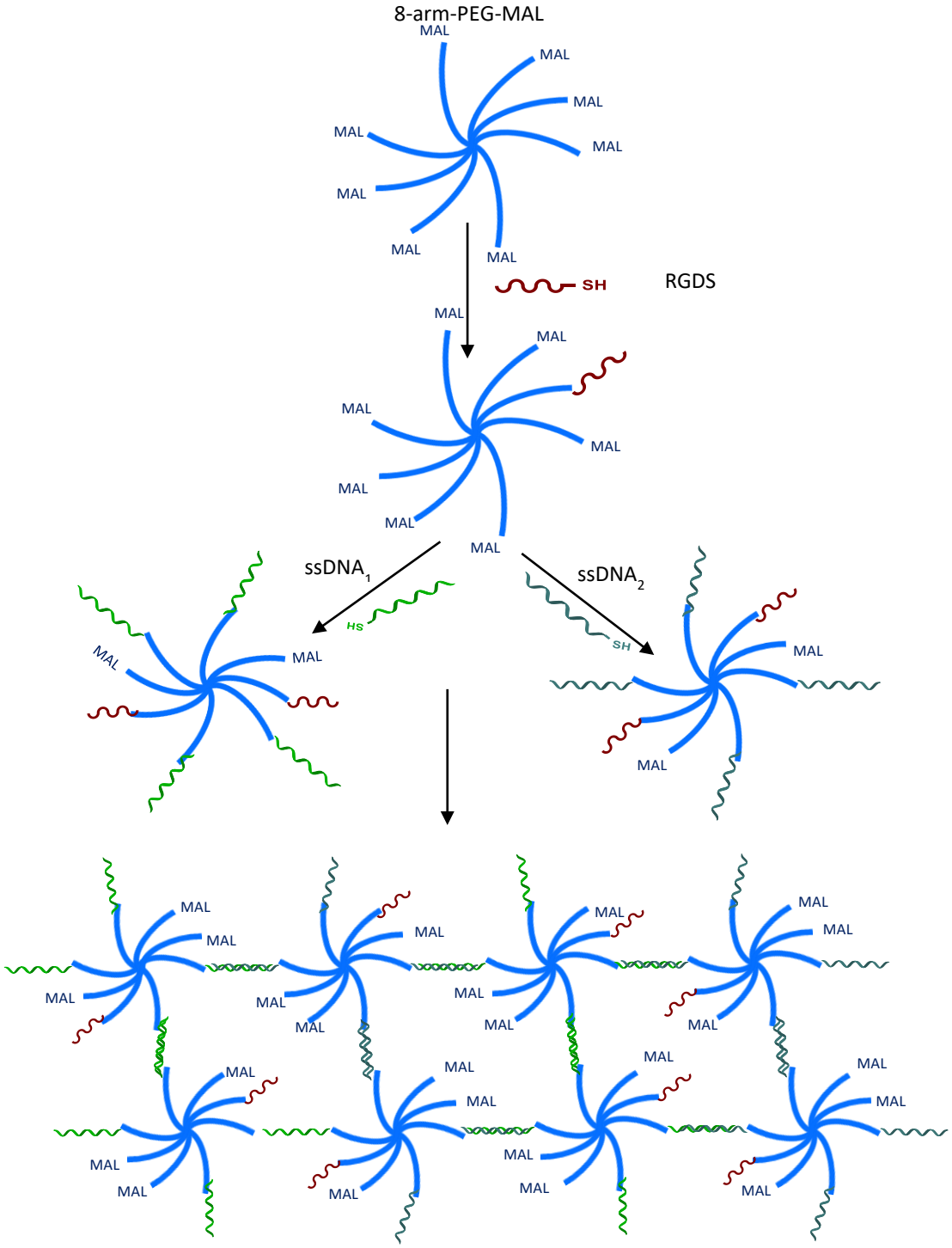

Figure 10 - Schematic view of the proposed self-assembled hybrid hydrogel based 8-arm PEG maleimide (PEG-MAL). Two complementary 20nt single stranded DNAs ($ssDNA_1$ and $ssDNA_2$) with a 5'-Thiol-group will be bound to PEG-MAL (40 kDa) through a thiol-MAL addition reaction. PEG-$ssDNA_{1/2}$ conjugates will be decorated with neurite-growth-permissive cell adhesive peptides synthesized with a cysteine, to confer bioactivity to the gels. For gel formation, precursor solutions of PEG-$ssDNA_1$ and PEG-$ssDNA_2$ will be mixed in stoichiometric amounts and cells encapsulated during sol-to-gel transition triggered by DNA hybridization.

2. ssDNA strands choice and hybridization

2.1. Selection of the ssDNA strands

The two complementary 20nt ssDNA sequences ($ssDNA_1$ and $ssDNA_2$) were *in silico* designed (Nupack software [104]) to avoid unwanted hybridization and formation of secondary structures, and to assure the thermodynamic stability of the hybridized sequence pairs under physiologic conditions (melting temperature above 55°C). Sequence 1 was 5'- /5ThioMC6-D/CGT CAC TGT CTT GCT GCA CG -3' (GC content: 60.0%, Mw: 6,388.4, Ext Coefficient: 174,400 L/(mole·cm)) and sequence 2 was 5'- /5ThioMC6-D/CGT GCA GCA AGA CAG TGA CG -3' (GC content: 60.0%, Mw: 6,504.5, Ext Coefficient: 199,600 L/(mole·cm)) were custom synthetized by Integrated DNA Technologies with a Thiol Modifier C6 S-S (disulfide) modification at the 5' end, in order to allow conjugation with PEG-MAL through SH-MAL addition reaction (Figure 11, [105]). The ssDNA sequences were bought with a standard desalting.

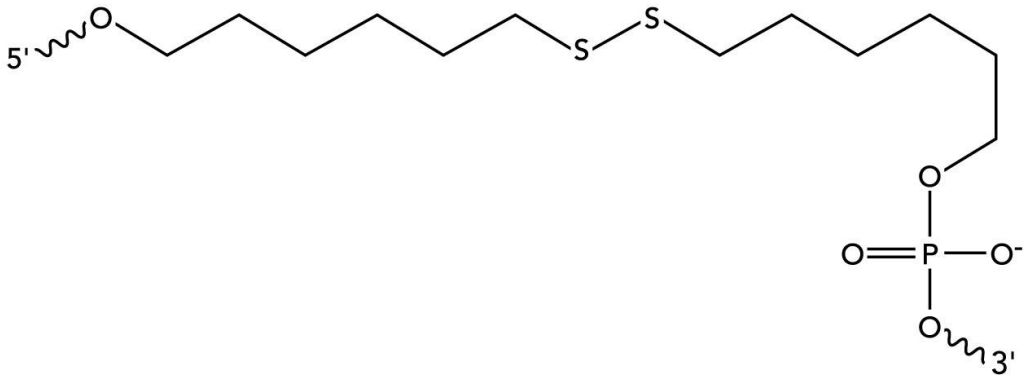

Figure 11. Scheme of Thiol Modifier C6 S-S (disulfide) modification at the 5' end. Image from IDT website [2]

2.2. Hybridization assessmente C6 S-S-ssDNA through PAGE

The C6 S-S-$ssDNA_{1/2}$ were re-suspended in nuclease free water (QIAGEN), at a concentration of 5 mM and stored in aliquotes of 50 µL at -20°C. The concetration was measured using Nanodrop spectrophotometer ND-1000 (Abs at 260 nm divided by the Ext Coefficient). Different ratios of C6 S-S-$ssDNA_1$ and of its complementary sequence (C6 S-S-$ssDNA_2$) were left to hybridize for 15 minutes before loading into PAGE in Tris/Borate/EDTA (TBE buffer - NZYTech). 5 pmoles of each strand were loaded with 1 µL of loading buffer and the electrophoresis run for 45 minutes at 90 V (10% resolving gel and 4% stacking gel). The gels were then stained with SYBRGold ® nucleic acid stain (Life Technologies) for 8-10 minutes and visualized using GelDock XR imager (BioRad). Calculations were performed with Image Lab 6.0.

3. Reduction and purification of C6 S-S-ssDNA sequences for deprotection of the reactive thiol.

3.1. Reduction of C6 S-S-ssDNA with TCEP

Reduction of C6 S-S-ssDNA (5 pmoles) by Tris-(2-Carboxyethyl) phosphine, Hydrochloride (TCEP, Thermo-Fischer) was assessed at different molar excesses (1,2×, 5×, 10×, 100×, 50 000×, 100 000× and 166 666×), during 2 hours. The efficacy of C6 S-S-ssDNA reduction was performed by PAGE.

3.2. Purification of TCEP-reduced thiol-terminated (SH-ssDNA ½)

BioRad P6 spin (BioRad) and Microspin G25 (GE Healthcare) were tested to perform the purification. The protocol performed for each purification column was accordingly to the recommended from the supplier.

P6 spin columns were centrifuged, three times, at 1 000 x (g) for 2 minutes with MilliQ water to exchange the buffer present in the column. After that, the reduced samples of SH-ssDNA ½ were placed directly to the center of the column and centrifuged for 4 minutes at 1 000 x (g). Following centrifugation, the samples are purified [106].

Before placing the reduced sample in the Microspin G25 column there is a need to prepare it. In order to do so, the resin must be re-suspended by vortexing. After that, spin the column for 1 minute at 735 x (g) to remove the excess and do it three more times with the desired buffer to exchange it. The sample was placed on the top-center of the resin and it was centrifuged 2 times at 735 x g. Following centrifugation, the samples were purified [107].

3.3. Reduction with DTT

To perform the reduction of the ssDNA strands with dithiothreitol (DTT), a molar excess of 125 000× (0.1 mM, pH 8.0) was used. The samples were left reducing overnight, for 2 hours and 1 hour.

3.4. Purification of DTT-reduced thiol-terminated (SH-ssDNA ½)

Purification was performed with Microspin G25 following the protocol explained before, and with Glen Gel Pack 1.0 mL (Glen Research). The column was first let to drain the excess of buffer and equilibrated afterwards with 15 mL of phosphate buffer 50 mM at pH 6.0. 750 µL of the sample was placed on the top frit of the column, and it was allowed for it to flow into the column bed. After that, 750 µL of phosphate buffer at 100 mM, pH 6, was added as pre-elution volume and 1000 µL of the same buffer was added as an elution volume [108]. After this step, the sample is purified. 2000 µL more was added.

When using the Glen Gel Pack 1.0 mL columns, the fractions were collected and analysed on the Nanodrop spectrophotometer ND-1000, by loading 1.5 µL of sample to visualize the spectrums on the software ND-1000 v3.5.2.

3.5. Presence of reactive thiols in SH-ssDNA

To detect the presence of reactive thiols in the fractions, the Measure-iT™ Thiol Kit (Lot No: 1924478, Invitrogen) was used according to supplier's instructions. Briefly, the samples (10 µL) were mixed with thiol-quantitation reagent and the fluorescence was measured (λ_{exc} = 494nm, λ_{em} = 517 nm) using a microplate reader (SynergyMx, Biotek) [109]. To determine the concentration of reactive thiols a concentration curve of glutathione was established.

4. Preparation and characterization of the PEG-RGDS conjugates

4.1. Assessment of reactive thiols in RGDS

To detect the presence of reactive thiols in RGDS, Measure-iT™ Thiol Kit was used as explained before.

4.2. Preparation of PEG-RGDS conjugates

The Ac-G<u>RGDS</u>P*C*-NH_2 (RGDS, where the cell binding sequence is underlined) peptide was synthetized at GenScript (Purity: 96.7%). 8-arm PEG-MAL was acquired from JenKem Technology (Mw: 37386 Da, Purity: 98.4%, Polidispersity: 1.05). RGDS conjugation to PEG-MAL was performed envisaging the functionalization of 1, 2, 4, 6 and 8 arms of PEG-MAL.

The maleimides from PEG are highly reactive with thiols, reacting stoichiometrically by Michael-type addition. Conjugation of RGDS to PEG-MAL was performed by reacting the thiol groups in RGDS with MAL groups in PEG-MAL. For this purpose, a 0.05 mM stock solution (pH = 6.0) of PEG-MAL and a 1 mM stock solution of RGDS (pH = 6.0) were prepared in MilliQ water, and the necessary volumes of stock solutions mixed by up-and-down. Immediately after mixing, the pH was adjusted to 7.5 by adding 0.1M NaOH. The conjugation reaction was performed at room temperature (RT) for 1 hour, under continuous stirring (200 rpm) and nitrogen (N_2) atmosphere. After the completion of the reaction, PEG-RGDS conjugates were then stored at -80°C for subsequent characterization.

4.3. Immobilization efficiency

The immobilization efficiency was assessed using Measure-iT™ Thiol Kit, as explained before.

4.4. HPLC analysis of PEG-MAL functionalization

The functionalization of PEG-MAL was followed by analytical High-Performance Liquid Chromatography (HPLC) (Hitachi High-Technologies Corporation, Transgeomic, Inc, Merck Hitachi model D700, software HSM), using a fixed concentration of PEG-MAL (0.2 mM). Two mobile phases were used, namely acetonitrile (ACN) (Sigma-Aldrich) with 0.05% trifluoroacetic acid (TFA) (Sigma-Aldrich) and MilliQ water with 0.065% TFA. The elution method consisted of 24.9 minutes at 5% ACN followed by three linear gradients: from 25.0' to 25.1': to 65% ACN; from 25.2' to 35.0': to 95% ACN and from 35.1' to 45.0': to 5% ACN in order to equilibrate the C-18 column (LiChrospher® 100 RP-18), at a constant flow of 1 mL/min. This method allows the C-18 column to have the desired performance in this type of assays.

5. Functionalization and characterization of 8-arm PEG-MAL with SH-ssDNA ½

5.1. Preparation of PEG-ssDNA conjugates

PEG-MAL functionalization was performed using purified SH-ssDNA ½, after determining the concentration of ssDNA in the Nanodrop spectrophotometer. Conjugation of SH-ssDNA to PEG-MAL was performed using stoichiometric balanced molar ratios of SH groups in SH-ssDNA to PEG-MAL of 2:1, 4:1 or 6:1, depending on the assays performed. Equal volumes of SH-ssDNA were added to PEG-MAL in order for the functionalization to occur, maintaining the ratio of SH:PEG-MAL of 2:1, 4:1 and 6:1, in order to functionalize 2, 4 or 6 arms of PEG-MAL. After vigorous stirring, the pH was adjusted to 7.5 (1M NaOH) to favour the reaction between the reactive thiol and the maleimide [110]. The samples were left reacting for 4 hours, at room temperature at 200 rpm, under N_2 atmosphere based on the work of Tsurkan *et al* (2013) [110]. After functionalization, the samples were stored at -80°C.

5.2. Immobilization efficiency

The incorporation of ssDNA into PEG-MAL was assessed using the Measure-iT™ Thiol Kit as described before. However, since SH-ssDNA used in the conjugation was in phosphate buffer (100 mM) and that of glutathione from the calibration curve was in MilliQ water, 1 µL of phosphate buffer (100 mM) or MilliQ water was added to each well of the 96-well plate containing the glutathione standard or the conjugate sample, respectively.

5.3. HPLC characterization of the formation of PEG-ssDNA conjugates

PEG-ssDNA conjugates formation was detected by analytical HPLC. HPLC was performed as described above. The measurements were performed at 290 nm, using a fixed concentration of PEG-MAL (0.1 mM).

5.4. Characterization of PEG-ssDNA conjugates by PAGE

To characterize PEG-ssDNA conjugates, a gradient-PAGE was performed (4-20% TBE gel, Invitrogen) in TBE buffer, for 30 minutes at 180V.

5.5. Purification and characterization of PEG-ssDNA conjugates by SEC

Preparative size exclusion gel filtration chromatography (SEC) was carried out at room temperature using AKTA PURIFIER FPLC system (GE Healthcare). Gel filtration was done using a Superose 6 10/300 GL column (GE Healthcare) equilibrated in 50% MilliQ and 50% phosphate buffered saline (PBS) buffer at 0.2 mL/min, using the wavelengths 230 nm, 260 nm and 290 nm. Fractions of 0.2 mL were collected. The functionalized sample was lyophilized and resuspended in PBS before loading it on the column.

6. Formation of PEG-RGDS-DNA hydrogels and rheologic analysis

PEG-MAL was reacted with 15 minutes with RGDS in order to allow the funtionalization of one arm, as explained before, after which, SH-ssDNA was added for functionalization of 4 arms of PEG-MAL. The samples were left to react for 4 h and then lyophilized and ressuspended with PBS at 5% w/v (weight per volume percentage). Subsequently, the Kinexus Pro Rheometer (Malvern) was used to examine the viscoelatic properties of the PEG-MAL-ssDNA hydrogels. Equal volumes of PEG-MAL functionalized with $ssDNA_{1/2}$ (2.5 µL each) were transferred to a plate-plate geometry (4 mm in diameter with sandblasted surface) previously set at 37°C, thoroughly mixed and allowed to polymerize *in situ* for 30 minutes under humidified atmosphere. A 10% compression was then applied to the gel to avoid slippage. For each condition, the linear

viscoelastic region (LVER) was first determined performing frequency sweeps (frequency: 0.01 to 10 Hz; strain: 2%). The storage modulus (G'), that measures the elastic energy stored during the deformation imposed by the rheometers oscillation, was determined and used as a measure of PEG-RGDS-DNA drops stifness. The loss modulus (G''), which translates into the energy dissipated by the PEG-RGDS-DNA drops during deformation was also recorded. Four drops were analysed under these conditions.

7. Preparation of fibrin hydrogels functionalized with HYD1 and AG73 cell adhesive sequences and rheologic characterization analysis

Fibrin hydrogels functionalized with peptides HYD1 (KIKMVISWKG) and AG73 (RKRLQVQLSIRT) were prepared as previously described [30], using the enzymatic cross-linking action of the transglutaminase factor XIIIa for peptide immobilization into fibrin. For this purpose, bi-domain peptides containing the sequence of interest at the carboxyl terminus and a factor XIIIa substrate from the NH_2-terminal sequence of α2-plasmin inhibitor (residues NQEQVSPL) at the amino terminus were synthesized at GenScript with a C-terminal amide (purity > 95%). Functionalized fibrin gels (50 µL) were formed by mixing equal volumes of a fibrinogen solution and a thrombin solution in TBS (pH 7.4) containing $CaCl_2$, aprotinin, and the bi-domain peptides [final concentration of Fb components: 6 mg/mL plasminogen-free fibrinogen from pooled human plasma containing factor XIII; 2 NIH U/mL thrombin from human plasma; 2.5 mM $CaCl_2$; 25 µg/mL aprotinin (all Sigma-Aldrich except for $CaCl_2$); 20 µM HYD1 bi-domain peptide; 60 µM bi-domain peptide AG73].

The storage (G') and loss (G'') moduli of unmodified and functionalized fibrin hydrogels were determined by rheometry using a Kinexus Pro Rheometer (Malvern Instruments), as described above.

8. 3D culture of h9-NSC within functionalized fibrin hydrogels

H9-derived human ES-NSC were purchased from Life Technologies and expanded according to the manufacturer's protocol (Gibco). To perform the cell embedment in fibrin, hES-NSPC were dissociated into single cells using StemPro® Accutase® and further suspended in fibrin gel (1×10^6 NSPC/mL). Human ES-NSCPs were initially cultured in StemPro® NSC serum-free media (SFM; Gibco) containing bFGF and epidermal growth factor (EGF) and, at day 2 of culture, the medium was switched to the mix StemPro® NSC SFM media:Neurobasal/B27 (1:1), without growth factors. The cells

were then dissociated into single cells and suspended in the fibrinogen solution prior to transferring the polymerizing solution to the wells of 6-well plates. Fibrin gels were allowed to polymerize for 30 min at 37°C in a 5% CO_2 humidified incubator, before the addition of cell culture media (800 µL/well). The cell-matrix constructs were cultured for 7 days in the presence of 5 µg/mL of aprotinin to delay fibrin gel degradation, following a protocol for neuronal differentiation [21].

9. En bloc F-actin/DNA fluorescence staining

F-actin/DNA fluorescence staining was performed *en bloc* in cell-fibrin constructs previously fixed in cell culture media containing 2% (v/v – volume per volume percentage) paraformaldehyde (PFA) (30 min at 37°C). Cell-fibrin constructs were permeabilized for 45 min with 0.2% (v/v) Triton X-100 at 50 rpm and blocked with 1% (w/v) bovine serum albumin (BSA) solution in PBS for 1 h. Cell-fibrin constructs were then incubated (overnight at 4°C) with Flash phalloidin Red 594 (BioLegend), under stirring (50 rpm), for visualization of filamentous actin (F-actin). After being rinsed trice with PBS, the samples were incubated for 1 h with 0.1 µg/mL of 4',6-Diamidino-2-phenylindole (DAPI, Sigma-Aldrich), also under stirring (50 rpm), for counterstaining of nuclei. The samples were washed with PBS buffer (three times at room temperature, for 5 minutes each), and finally mounted in Fluoromount™ mounting media (Sigma-Aldrich). Processed samples were stored at 4°C in the dark until observation under the confocal laser scanning microscope [CLSM; Leica TCS SP5 II (Leica Microsystems, Germany)]. The volumes used were between 200 to 400 µL for each well of 24-well plate.

10. Statistical analysis

Data was treated using BM SPSS Statistics Software as well as GraphPad Prism (version 7). Normality of data was tested using Shapiro-Wilk test and confirmed with quantile-quantile plots. Statistically significant differences between two conditions were detected using the Student's independent-samples t-test. Two-tailed significance levels were considered, and results found statistically significant when $p < 0.05$.

CHAPTER III

RESULTS AND DISCUSSION

1. Hybridization of ssDNA strands

The selected ssDNA strands were chosen since they present a high temperature melting point (59.0 °C) as well as a low number of G-C and A-T bonds, an example scheme can be seen in Figure 12.

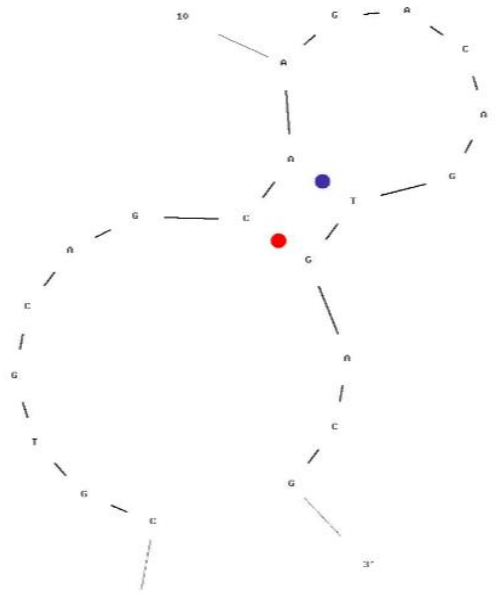

Figure 12. Most likely conformation of the two 20nt ssDNA sequences used. C-G bond is represented by the red dot, and A-T bond is represented by the blue dot. Image reproduced from the Specification Sheet provided by the manufacturer of the strands, IDT.

The ssDNA sequences strands were synthetized with a thiol modifier (5' Thiol Modifier C6 S-S), to allow subsequent conjugation with PEG-MAL. The disulfide bond in the 5' Thiol Modifier C6 S-S protects the thiol groups from reacting with themselves. This modification is commonly used when shipping oligonucleotides in order to prevent spontaneous and uncontrolled oxidation of thiol groups, which could lead dimer formation and useless oligonucleotides [111].

Firstly, the hybridization of the two C6 S-S-ssDNA sequences was assessed. To accomplish that, PAGE under non-reducing conditions was performed, using the same number of moles of each strand. The result can be seen in Figure 13.

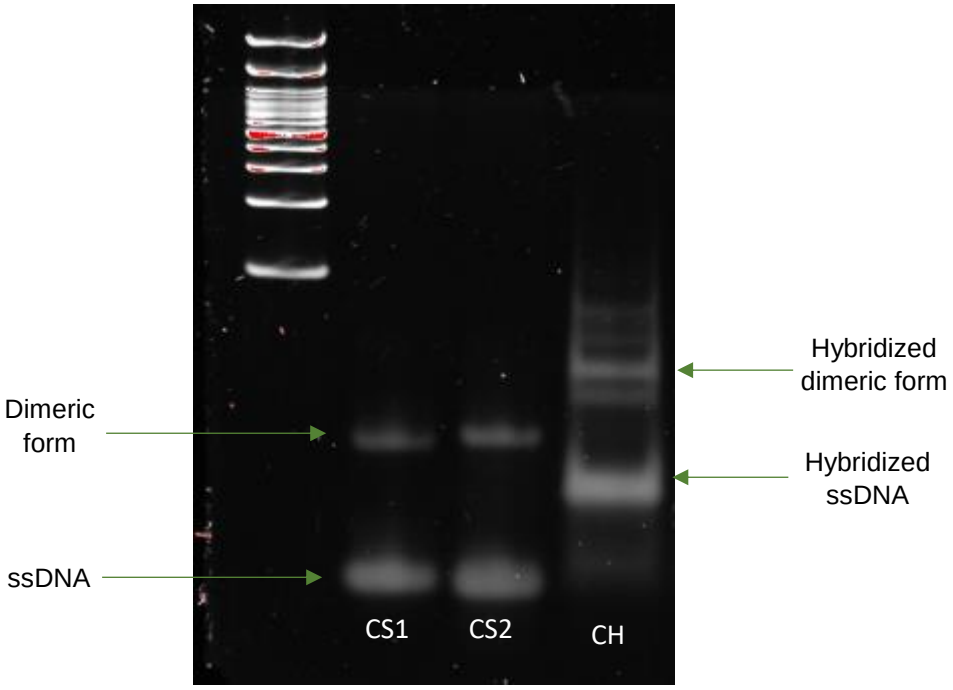

Figure 13. PAGE of the two C6 S-S-ssDNA sequences after hybridization (without prior reduction of the disulfide bond). CS1 and CS2 showC6 S-S-ssDNA sequence 1 and 2, respectively (controls). CH represents the hybridized C6 S-S ssDNA sequence. It is possible to see that the two C6-S-S ssDNA sequences hybridize. However, there is still some remaining ssDNA that did not react. Also, both controls (CS1 and CS2) present a second band assigned to a dimeric form of C6 S-S ssDNA most possibly produced during the synthesis of the thiol-modified ssDNA sequences.

It is possible to see, from Figure 13, that the two C6-S-S-ssDNA sequences (controls) show two bands instead of just one, as it would be expected. This can be due to the presence of a dimeric form of ssDNA formed as a by-product during the thiolation modification reaction, due to the establishment of an internal disulfide bond.

With hybridization there is the formation of a band with a higher molecular weight than the C6 S-S-ssDNA controls (runs less on the polyacrylamide gel), as expected. However, it is still possible to see a fade band with a molecular weight similar to that of the individual ssDNA sequences, which indicates the use of an excess of ssDNA. Moreover, this band can also be associated to the presence of non thiolated ssDNA. As a result, various hybridization ratios were tested, varying strand 1 or 2 (Figure 14 and 15).

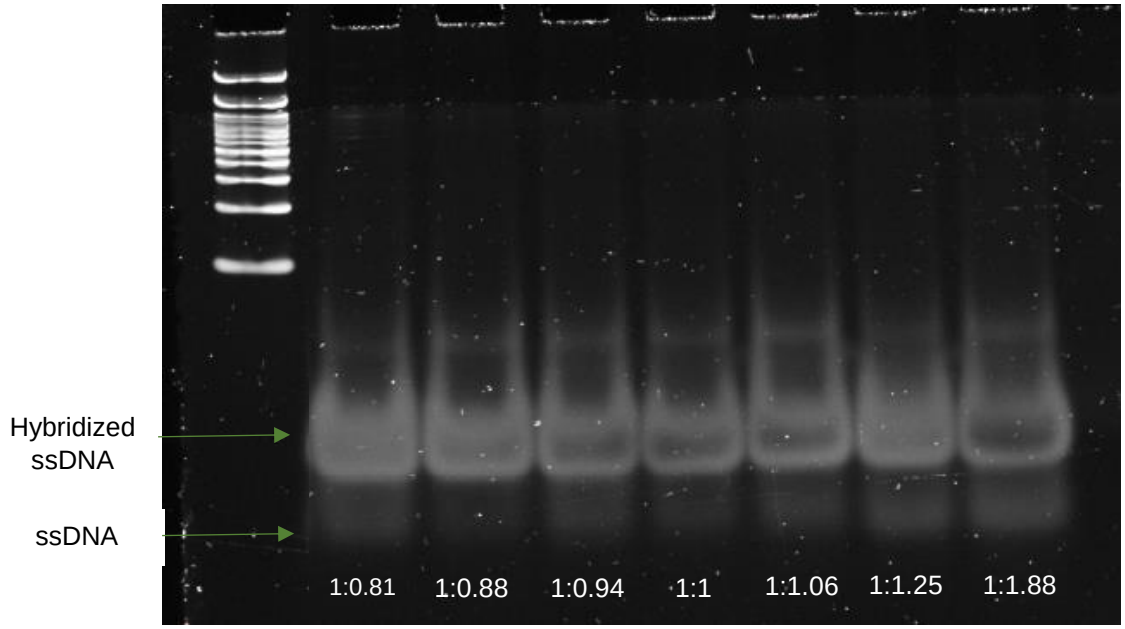

Figure 14. Assessment of the best ratio for hybridization of ssDNA sequences 1 and 2. Several ratios of C6 S-S-ssDNA 1 and 2 were tested, keeping the concentration of C6-S-S-ssDNA sequence 1 constant. Results suggest that the hybridization of the two ssDNA sequences is more efficient than a ratio of 1 mol of $ssDNA_1$ s to 0.88 moles of $ssDNA_2$.

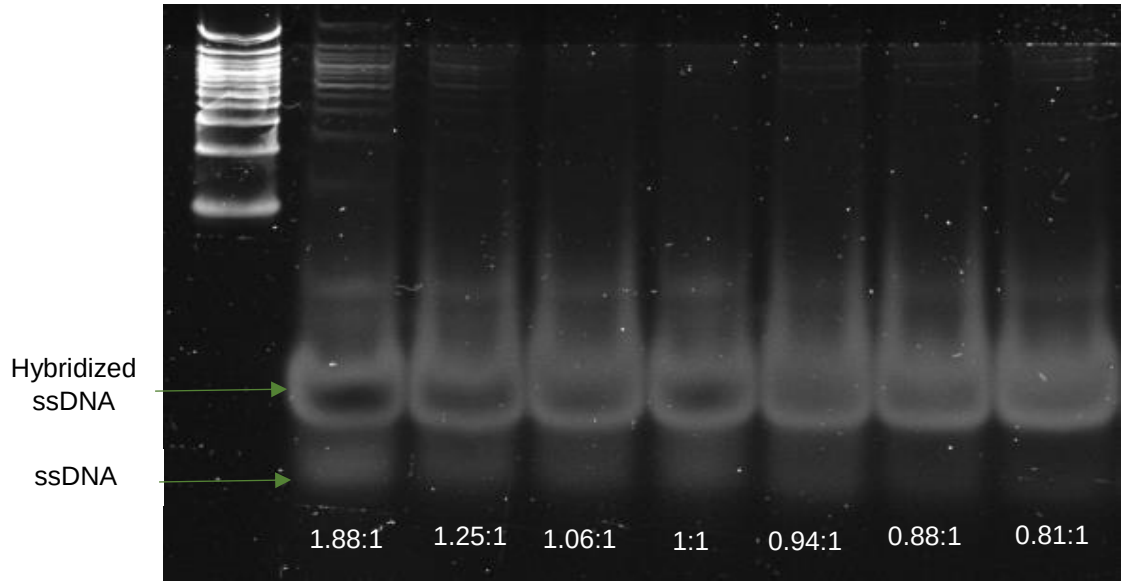

Figure 15. Assessment of the best ratios for hybridization of ssDNA sequences 1 and 2. Several ratios of C6 S-S-ssDNA 1 and 2 were tested, keeping the concentration of C6 S-S-ssDNA sequence 2 constant. Results suggest that the hybridization of the two ssDNA sequences is more efficient at a ratio of 1 mol of $ssDNA_2$ and 0.88 or0.81 moles of $ssDNA_1$.

After seeing that the best $ssDNA_1$:$ssDNA_2$ ratios were those of 1:0.88, 0.88:1 and 0.81:1, PAGE was performed to test these ratios and estimate the correspondent percentage of non-reactive ssDNA (Figure 16). Semi-quantitative image analysis of the gels with Image Lab 6.0, revealed that with equimolar amounts of ssDNA complementary sequences, the percentage of non-reactive ssDNA attains 2.51%. Among the ratios tested, the lowest percentage of non-reactive ssDNA (1.19%) was obtained using a 0.88:1 molar ratio of ssDNA strand 1 to ssDNA strand 2.

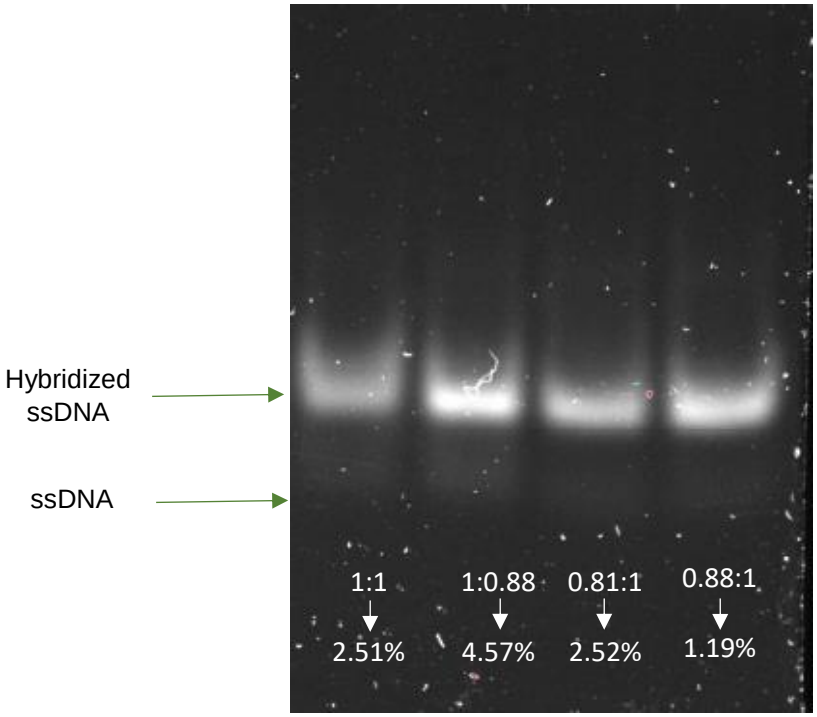

Figure 16. Assessment of the best ratios for hybridization of ssDNA sequences 1 and 2and semi-quantitative analysis of the percentages of unreacted ssDNA.

2. Optimization of C6 S-S-ssDNA reduction and purification

The reduction of the disulfide bond of C6 S-S-ssDNA for deprotection of the thiol reactive group was subsequently performed by two different reducing agents. In the presence of reducing agents, one molecule of the reducing agent undergoes disulfide exchange, by cleaving the disulfide bond and forming a new, mixed one. Then, a second

molecule of the reducing agent cleaves the mixed disulfide, forming a molecule of the oxidized reducing agent (Figure 17) [112].

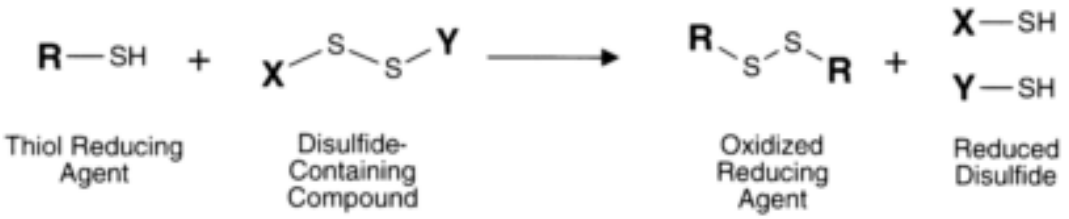

Figure 17. Scheme of the reaction between thiol reducing agents and the disulfide containing compound. Image reproduced from Hermanson et al (2015) [112]

There are well-established reducing agents that can reduce this disulfide bond into the active sulfhydryl form, such as tris(2-carboxyethyl) phosphine hydrochloride (TCEP) and dithiothreitol (DTT). Both of them are only able to perform partial reduction, corresponding to the most accessible disulfides [113]. According to Faucher and Grand-Maître (2006), the reduction of several functional groups with TCEP, presented a yield from 0% to 99%. Still, the yield of disulfide reduction by TCEP in the case of C6-S-S-ssDNA is not described [114]. TCEP is a thiol-free reducing agent, easily soluble and very stable in various aqueous solutions. It can reduce disulfide bonds at lower pHs, it's more stable and more effective than DTT [115]. DTT, however, has low redox potential reducing the disulfides, while maintaining the free thiols in solution even in the presence of oxygen [113]. Both reduction methods are depicted in Figure 18 and 19 [113, 115].

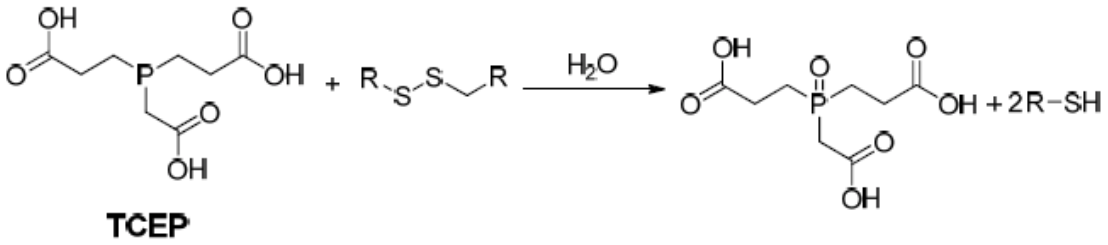

Figure 18. Scheme of the reaction of TCEP with disulfide containing compounds. Image reproduced from ByoSynthesis [113].

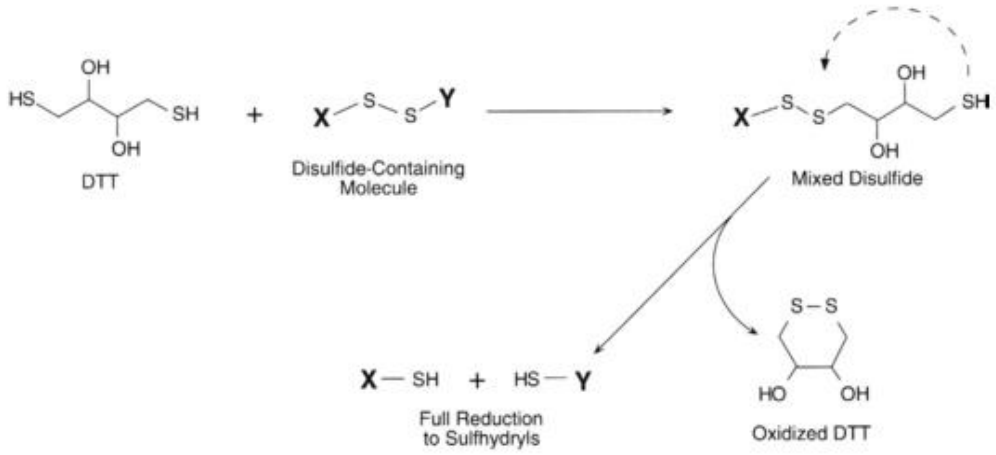

Figure 19. Scheme of the reaction of DTT with disulfide containing compounds. Image reproduced form Hermanson et al (2013) [99].

2.1. Reduction/Purification with TCEP

Due to the absence, in TCEP, of thiol groups which could eventually compete with SH-ssDNA for binding to PEG-MAL, and its higher reported efficiency for disulfide reduction as compared DTT (2-3% more efficient), TCEP was initially selected for reduction of C6 S-S-ssDNA sequences. Reduction efficacy was initially followed by nondenaturing PAGE, as disulfide reduction was expected to be translated into a decrease of the intensity of the band correspondent to the dimeric form of ssDNA. Table 2 depicts the conditions tested for disulfide reduction by TCEP and the resultant products as assessed by PAGE (Supplementary Information SI 1 and Figure 20) [113].

Table 2 - Conditions tested for the reduction of the disulfide bond in C6 S-S-ssDNA with TCEP,

[C6 S-S SSDNA] (µM)	REDUCING AGENT	MOLAR EXCESS OF REDUCING AGENT	PH	TIME OF REDUCTION (H)	OBS
1	–	–	–	–	Dimeric form and ssDNA correspondent bands appear
1	TCEP	1.2	2.5	2	Similar intensity of the bands
1	TCEP	5	2.5	2	Similar intensity of the bands
1	TCEP	10	2.5	2	Similar intensity of the bands
1	TCEP	100	2.5	2	Similar intensity of the bands
1	TCEP	100 000	2.5	2	The Amount of TCEP interfered with the gel (Fig. 18)

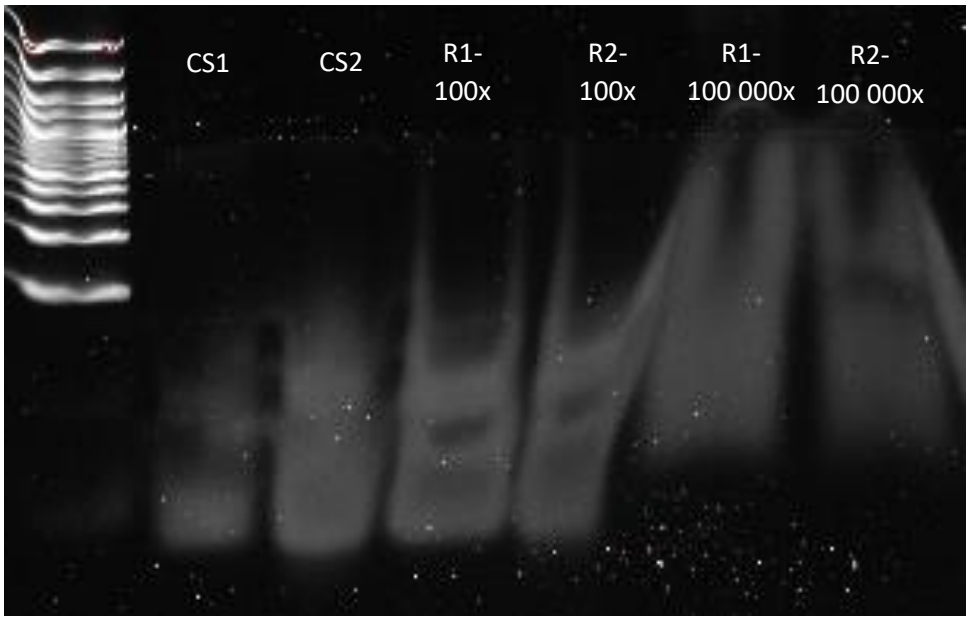

Figure 20. Efficacy of the reduction of the disulfide bond in C6 S-S-ssDNA with TCEP with a 100× and 100 000× molar excess for 2 hours. CS1 and CS2 corresponds to C6 S-S-ssDNA sequence1 and 2, respectively (controls); R1-100× and R1-100 000× shows C6-S-S-ssDNA$_1$ reduced with a 100× and 100 000× molar excess of TCEP, respectively; R2-100× and R2-100 000× depict C6 S-S-ssDNA$_2$ reduced with 100× and 100 000× molar excess of TCEP. When reduced using the highest molar excess, TCEP reacted with the PA gel.

For molar excess ratios of TCEP lower than 100×, no significant changes in the intensity of the upper band (correspondent to the dimeric form of thiolated ssDNA) were detected. Moreover, we observed that the excess of TCEP was interfering with the PA gel. In fact, the cleavage of internal disulfide bonds in ssDNA has been reported to be more challenging when compared to that of terminal disulfide bonds [116]. As the change in the molecular weight of C6 S-S-ssDNA after disulfide cleavage cannot be detected by PAGE, we pursued with the purification of TCEP-treated C6 S-S-ssDNA.

Purification of the TCEP-reduced C6 S-S-ssDNA was performed to eliminate:

- ➔ TCEP, recently described to be able to react with MAL groups and, therefore, potentially compete with ssDNA for binding to PEG-MAL [117];
- ➔ The thiolated by-product (C6-SH) formed by reduction of disulfide bonds in C6 S-S-ssDNA [115].

The conditions used to obtain purified and reduced C6 S-S-ssDNA are shown in Table 3. Due to the high molar excesses of TCEP used to reduce C6 S-S-ssDNA, PAGE was performed to detect TCEP in the purified products, due to its ability to react with PA gels. When using Biorad P6 Spin columns, no band was detected, possibly due to the cut off of the column (6 kDa) being very close to that of ssDNA. When using Microspin G25 purification columns (> 10 bases), DNA was detected. However, the band was distorted which suggests the presence of TCEP. Disulfide reduction of C6 S-S-ssDNA with DTT was, subsequently, performed.

Table 3 – Conditions tested to obtain purified C6 S-S-ssDNA reduced with TCEP

[C6 S-S-SSDNA] (µM)	REDUCING AGENT	MOLAR EXCESS OF REDUCING AGENT	PH	REDUCTION TIME (H)	PURIFICATION COLUMN	BUFFER	OBS
2	TCEP	50 000	2.5	2 hours	Biorad P6 Spin	–	DNA was not detected
2	TCEP	50 000	2.5	2 hours	Microspin G25	Autoclave MilliQ	Distorted band

2.2. Reduction/Purification with DTT

PAGE analysis of reduction of C6 S-S-ssDNA by DTT, overnight, showed a clear single band (Table 4 and Figure 21), indicating the cleavage of the dimeric form and, therefore, successful reduction of the C6 S-S-ssDNA. The time required for disulfide

bonds can be possibly further reduced, since at a pH between 7.0 and 8.1 and at molar excesses of 125 000x, one hour is sufficient for disulfide bond reduction [113]. Furthermore, PAGE analysis is widely used to follow DTT disulfide bond reduction [118].

Table 4 - Condition tested for reduction of the disulfide bond in C6 S-S-ssDNA with DTT

[C6 S-S-SSDNA] (µM)	REDUCING AGENT	MOLAR EXCESS	PH	TIME OF REDUCTION	OBS
0.8	DTT	125 000 (0.1 M DTT)	8.0	Overnight	Single Band

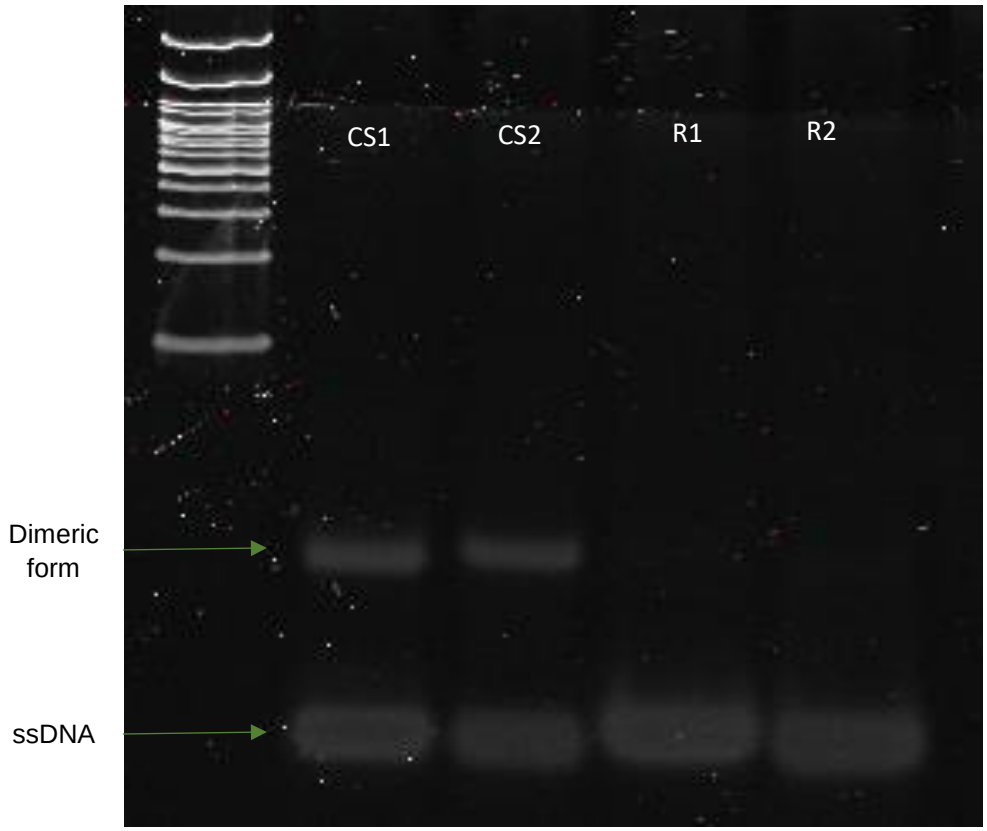

Figure 21. Efficacy DTT reduction of C6 S-S-ssDNA disulfide bond. R1 and R2 represents the reduction result of ssDNA strand 1 and 2, respectively. CS1 and CS2 corresponds to C6 S-S-ssDNA sequence 1 and 2, respectively (controls).

Purification of the DTT-reduced C6 S-S-ssDNA was performed to eliminate:

- ➔ DTT, which presents, in its reduced form, two thiols able of reacting with MAL groups from PEG-MAL;
- ➔ The thiolated by-product (C6-SH) formed by reduction of disulfide bonds in C6 S-S-ssDNA [115].

Purification using Microspin G25 columns showed reduced and highly variable recovery yield, as assessed using the Nanodrop, which was also dependent on the ssDNA sequence (Table 5). When using DTT at this molar excess, we cannot exclude the contamination of purified SH-ssDNA with DTT. Especially when using centrifuge columns, since there is no control over the elution.

Table 5. Recovery yield of purified SH-ssDNA using Microspin G25 columns, when loading the purification column with different concentrations of DTT-reduced C6 S-S-ssDNA. The yield is expressed as percentage. Results correspondent to a [ssDNA] of 0.5 mM are the mean ± SD of 5 purifications.

[ssDNA]	0.015 mM	0.5 mM	0.6 mM	2.5 mM
ssDNA 1	35.09 %	58.33 ± 39.74	73.86 %	8.69 %
ssDNA 2	27.43 %	55.43 ± 38.08	77.33 %	66.73 %

In order to improve the recovery yield, Glen GelPak 1.0 mL gravity columns were subsequently used, due to their specificity for DTT removal. Eluted fractions were analysed in the Nanodrop. Prior to reduction C6 S-S-ssDNA ½ presents a peak at 260 nm (DNA), and a small shoulder at 230 nm, assigned to disulfide bond. According to Yang. F. (2015), reduced but unpurified SH-ssDNA has an absorbance at 220 nm and 260 nm, and reduced and purified SH-ssDNA adsorbs at 210 nm and 260 nm [119]. Also, reduction by-products with free thiols have a single absorbance peak at 230 nm [119]. DTT, due to his ring structure, presents a peak at 283 nm in the oxidized form (after reacting), and a peak at 209 nm in the reduced form [120, 121]. Since the spectrophotometer used to analyse the spectra (Nanodrop) could not measure wavelengths lower than 220 nm, the presence of purified reduced SH-ssDNA was detected at 220 nm.

A representative spectrophotometric analysis (using Nanodrop) of the fractions eluted from the purification column is presented in Figure 22.

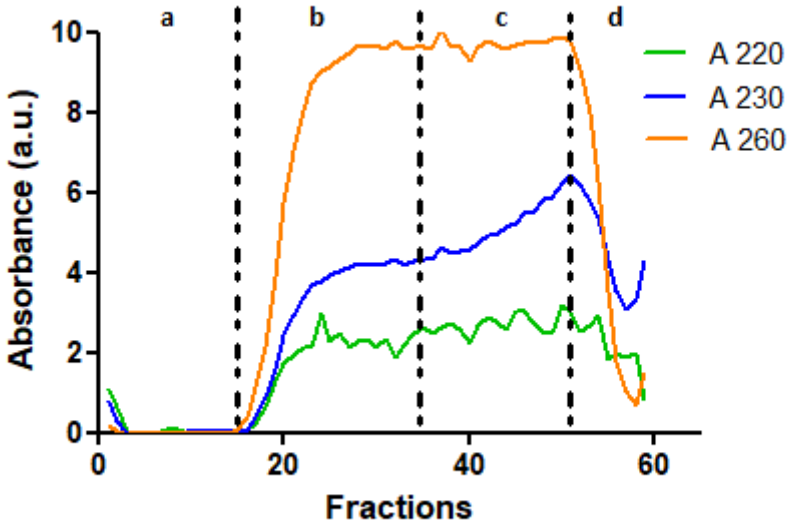

Figure 22. Absorbance of the fractions eluted from the purification column previously loaded with DTT-reduced C6 S-S-ssDNA$_2$, as assessed using the Nanodrop spectrophotometer. Section a corresponds to the pre-elution volume and, as such, to phosphate buffer. Section b corresponds to the elution volume and contains reduced and purified SH-ssDNA. The addition of more buffer allowed the recovery of more fractions (Section c) revealing increased absorbance at 230 nm, attributed to the elution of small by-products of DTT reduction containing free thiol groups. Section d corresponds to the elution of oxidized DTT. Absorbance at 220 nm (A 220) is represented in green. Absorbance at 230 nm (A 230) is represented in blue. Absorbance at 260 nm (A 260) is represented in orange.

Section (a) of Figure 22, corresponds to the pre-elution volume and therefore to fractions containing only buffer. A typical absorbance spectrum can be seen in Figure 23 a). The following eluted fractions correspond to the elution volume and present an absorbance peak at 260 nm, which was attributed to SH-ssDNA (section b, Figure 22). These eluted fractions also present a small absorbance peak at 230 nm, most possibly correspondent to non-reduced oligonucleotides. A typical sample from this section has the following spectrum (Figure 23 b)). The addition of more phosphate buffer to the column, besides that correspondent to the elution volume, allowed the recovery of more fractions (section c, Figure 22). A representative absorbance spectrum of these fractions (Figure 23 c)), depicts an increased absorbance at 230 nm, as expected due to the elution of the thiolated by-product (C6-SH). As these could compete with SH-ssDNA for binding to MAL groups from PEG-MAL, these fractions could not be used for functionalization of PEG-MAL. Close to the end, the absorbance of the eluted fractions at 260 nm was drastically reduced, indicating that SH-ssDNA was no longer present in

these fractions. These revealed an increased absorbance at 230 nm (Figure 23 d), attributed to the DTT reduction thiolated by-product (C6-SH), as above described (section d, Figure 22). Also, near the end of the measurements, an increase in the absorbance at high wavelengths was possibly due to the elution of oxidized DTT.

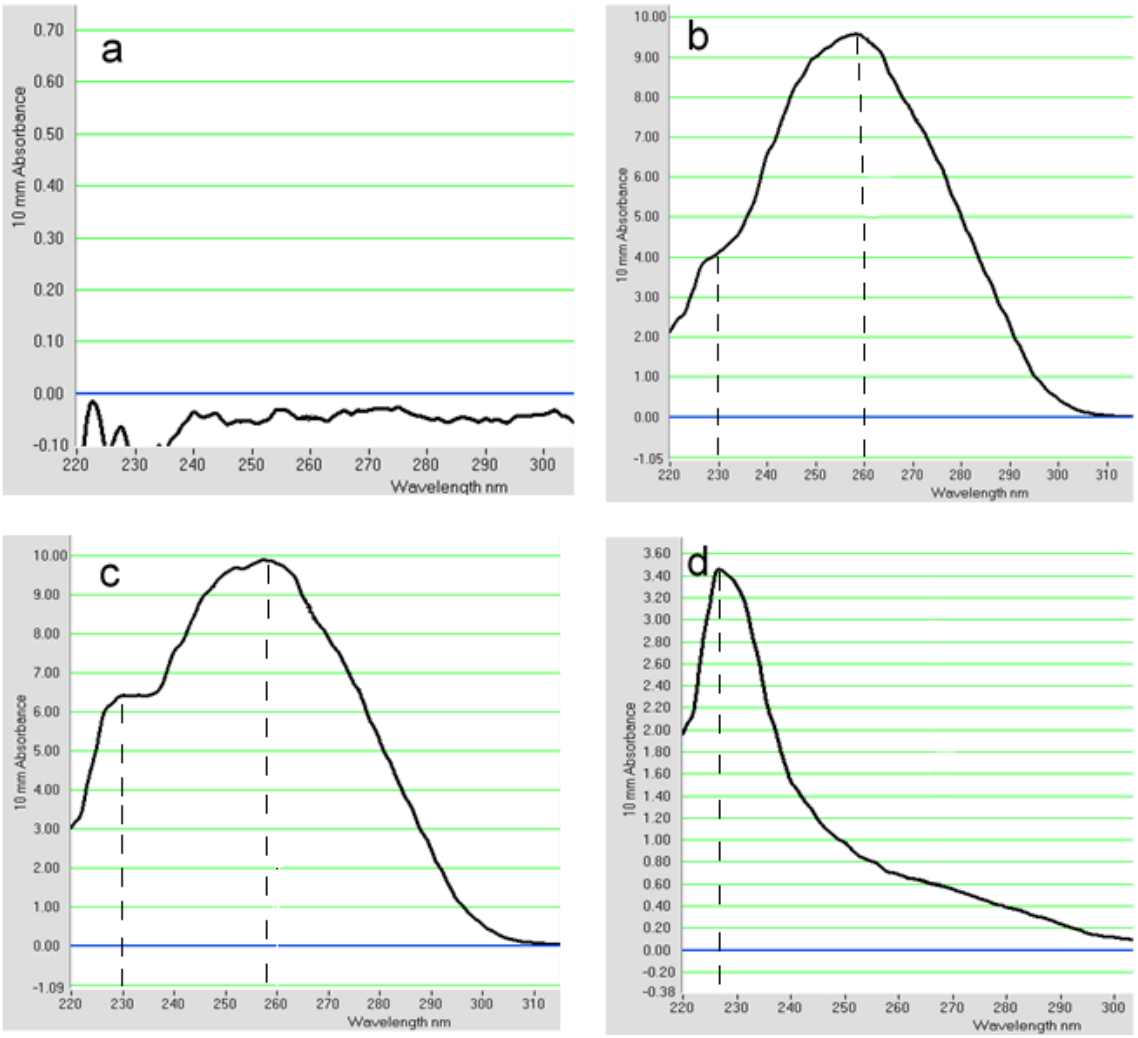

Figure 23. Typical absorption spectrum correspondent to a) pre-elution phosphate buffer; b) elution volume with an absorbance peak at 260 nm, attributed to SH-ssDNA, there is also a small absorbance peak at 230 nm, that can correspond to non-reduced oligonucleotides; c) increased absorbance at 230 nm, correspondent to the elution of the thiolated by-product (C6-SH); d) absorbance peak at 230 nm correspondent to DTT reduction thiolated by-product (C6-SH)

In brief, spectrophotometric analysis at 220, 230, and 260 nm, showed that Glen Gel Pak gravity columns could be successfully used to isolate reduced ssDNA from DTT reduction by-products. The fractions containing purified reduced SH-ssDNA were pooled, and the recovery yield was quantified. SH-ssDNA$_1$ sequence revealed a lower

recovery yield than SH-ssDNA $_2$ (Table 5), indicating that SH-ssDNA purification through this purification column is sequence dependent due to a differential interaction with the column gel.

Table 6. Recovery yield of purified SH-ssDNA and that of total ssDNA with Glen GelPak 1.0 mL columns, when loading the purification column with 0.2 mM of DTT reduced C6 S-S-ssDNA. The yield is expressed as a percentage results presented as mean ± SD.

	Purified SH-ssDNA (n = 2)	**Total ssDNA (n = 5)**
ssDNA 1	25.42 ± 13.26	37.69 ± 10.60
ssDNA 2	65.01 ± 1.22	91.50 ± 6.08

2.3. Percentage of reactive thiols in purified reduced ssDNA

The ssDNA concentration was measured, and the percentage of free thiols in SH-ssDNA was determined using the Measure-iT™ Thiol Assay Kit [65]. This assay is a very sensitive method for detection of free thiols, as it can detect down to 0.05 μM of free thiols, making it "400 times more sensitive than colorimetric assays based on Ellman's reagent [122], [123]. The fractions containing purified reduced SH-ssDNA were pooled, ssDNA concentration was measured, and the percentage of free thiols in SH-ssDNA determined using the Measure-iT™ Thiol Assay Kit [65]. The percentage of free thiols varied with the sequences as is presented in Table 7. The low percentage of free thiols was attributed to the presence of a residual amount of the dimeric form of ssDNA, detected by Nanodrop spectrophotometer (Section 2.2, Figure 23b), although this was not perceive by PAGE analysis (Section 2.2, Figure 21). Moreover, as for this study, ssDNA was acquired without purification, which can indicate the presence of non-thiolated ssDNA that might have also contributed to low percentage of free thiols. Of note, this could contribute the differential behaviour of the two ssDNA strands.

Table 7. Percentage of reactive thiols after reduction with DTT, obtained by Measure-iT™ Thiol Assay Kit. Results are shown in percentage, mean ± SD (n=3)

	% of free thiols
ssDNA strand 1	44.89 ± 5.30
ssDNA strand 2	76.33 ± 2.61

3. Preparation and characterization PEG-MAL-RGDS conjugates

GRGDSPC (cell binding sequence underlined) was immobilized into 8-arm PEG-MAL to confer bioactivity to the proposed PEG-MAL DNA-crosslinked hydrogel. RGDS is a cell-adhesive motif with neurite outgrowth ability present in fibronectin, widely explored to confer bioactivity to hydrogels for neural applications (Table 1) [90, 94, 124, 125]. This domain is mainly recognized by α5β1 integrin, but also by αvβ3, αvβ1, αvβ5, αvβ6 and α8β1 [86, 126].

RGDS was conjugated to PEG-MAL through Michael-type addition (Figure 24). This reaction can be initialized by various nucleophiles, in this case -SH [127].

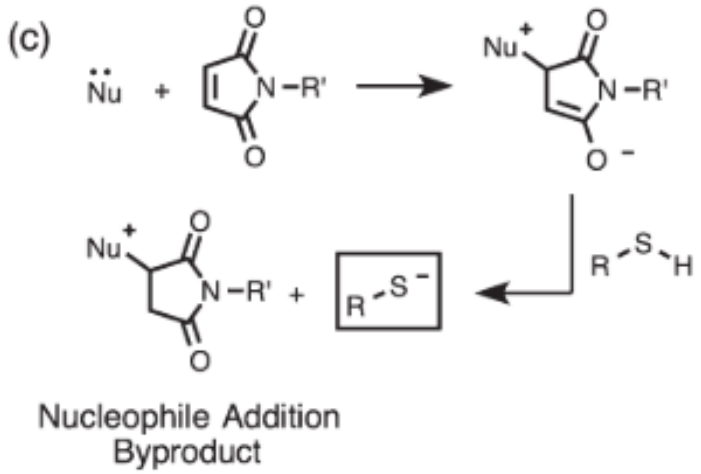

Figure 24. Scheme of Michael type addition reaction. Image from Northrop et al (2015) [126]

Thiol-maleimide reactions are highly reliable, efficient and selective, being the primary mean of bioconjugation for decades [127]. Therefore, the percentage of reactive thiols in "as received" RGDS was determined using the Measure iT™ Thiol Assay Kit. Results revealed that 84.48 ± 1.10 % (n = 9) RGDS molecules were carrying a thiol reactive group. RGDS was added to PEG-MAL using stoichiometric balanced molar ratios of 1:1 to 8:1 of SH groups in RGDS to PEG-MAL, in order to functionalize 1 to 8 arms of the multi-arm PEG. The solution was vigorously mixed to allow low polydispersity of the formed conjugate. Subsequent elevation of the pH resulted in the enhanced nucleophilicity of thiol groups, fasting the reaction between the cysteine and maleimide [110].

3.1. RGDS Immobilization Efficiency

The immobilization efficiency was assessed quantifying the concentration of free thiols at the end of the reaction, using Measure iT™ Thiol Assay Kit. The resulting immobilization efficiency is presented in Table 8. A high immobilization efficiency was

attained independently of the molar ratio of SH:PEG-MAL used. Interestingly, when preparing 4-arm PEG-RGDS conjugates, Phelps et al (2012) reported a decrease in peptide immobilization efficiency when increasing the molar ratio of SH:PEG-MAL [65], a tendency which we did not observe. Still, in contrast to our study, the two precursor solutions were mixed at a pH of 7.4.

Table 8. Quantification of thiols remaining after 8-arm PEG macromer functionalization with RGDS, as a function of the SH:PEG-MAL molar ratio. Results are the mean ± SD (*n* = 3).

SH:PEG-MAL ratio	Input [SH] (μM)	[Unreacted SH] (μM)	Immobilization efficency (%)
1:1	43	2.56 ± 0.11	94.06 ± 0.27
2:1	83	3.81 ± 0.53	95.41 ± 0.78
4:1	166	12.09 ± 0.97	92.72 ± 0.59
6:1	249	47.64 ± 1.83	80.87 ± 0.74
8:1	400	25.21 ± 5.95	92.46 ± 1.87

3.2. HPLC characterization of PEG-MAL functionalization

The functionalization of MAL groups from 8-arm MAL terminated PEG- was followed by analytical HPLC. HPLC consists in the interaction of the sample with the non-polar solid phase (column) and the polar mobile phase. As a result, the lower the solute (sample), the higher its retention time [128, 129]. Acetonitrile was used for the mobile phase, due to its low UV-absorbance, and, as a consequence, low background noise [129]. The wavelength used was 290 nm for all the measurements, to detect changes in the maleimide group in PEG-MAL (specific maleimide UV-absorbance peak) [110]. Results are present in Figure 25. With the increase molar ratio of SH:PEG-MAL, a reduction of the retention time was consistently observed, indicating a higher affinity of RGDS-functionalized PEG arms to the mobile phase, possibly due to its increased polarity. Also, a decrease in the absorbance intensity at 290 nm was observed when increasing the SH:PEG-MAL molar ratio (except for 8:1). Both these observations, namely the change in the retention time as well as the reduction of the absorbance at 290 nm, indicates successful functionalization of MAL groups. At this wavelength, RGDS is not detected (Supplementary Information S2).

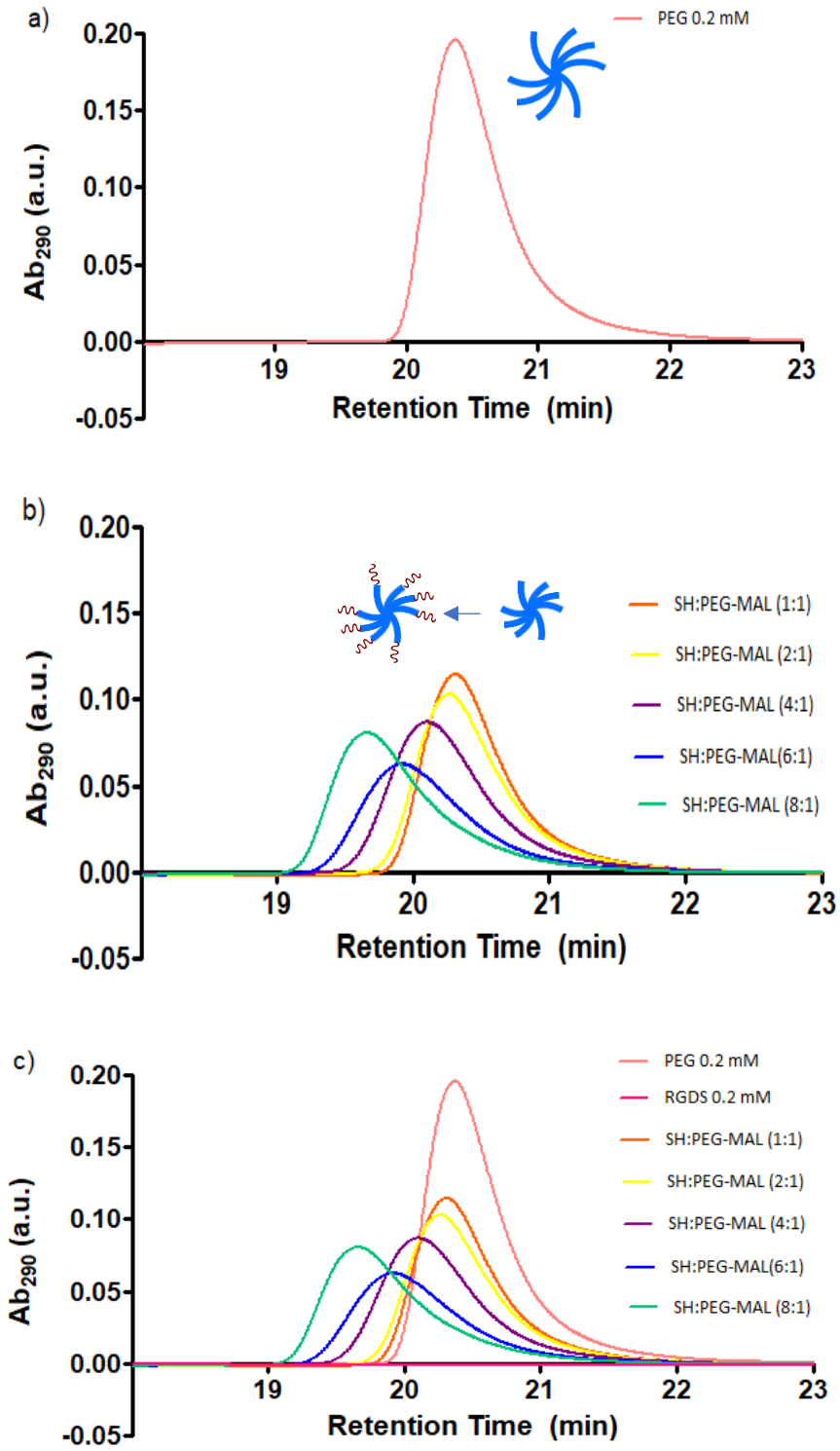

Figure 25. Chromatographic analysis of PEG-MAL functionalization, using a detection wavelength of 290 nm. HPLC chromatogram of: A) PEG; B) RGDS; C) Reaction mixture of PEG-MAL with RGDS using different SH:PEG-MAL molar ratios. For each condition, the average of 2 chromatograms is shown.

4. Functionalization of PEG-MAL with ssDNA

PEG-MAL functionalization with SH-ssDNA was performed by adding SH-ssDNA to PEG-MAL using stoichiometric balanced molar ratios of 4:1 of SH groups in SH-ssDNA to PEG-MAL, in order to functionalize 4 arms of the multi-arm PEG. This crosslinking ratio leaves 4 reactive arms available for the binding of neurite-promoting cell adhesive peptides.

4.1. Immobilization Efficiency

Immobilization efficiency was assessed quantifying the concentration of unreacted thiols remaining after the functionalization of the multi-arm PEG-MAL, using Measure-iT™ Thiol Assay Kit. The concentration of unreacted thiols found was below the limit of detection of the kit (0.5 µM), which indicates an immobilization efficiency higher than 97.33 ± 0.12 % (Table 9).

Table 9. Quantification of thiols remaining after 8-arm PEG macromer functionalization with $ssDNA_2$, as a function of the SH:PEG-MAL molar ratio. Results are the mean ± SD (n = 3).

SH:PEG-MAL ratio	Input [SH] (µM)	[Unreacted SH] (µM)	Immobilization efficiency (%)
4:1	18.7	2.67 ± 0.02	97.33 ± 0.12

4.2. HPLC analysis of the formation of PEG-ssDNA conjugates

Analytical HPLC was used to detect the formation of PEG-ssDNA conjugates. To follow the functionalization of MAL groups from PEG-MAL, detection was performed at 290 nm. An additional advantage of this wavelength is its ability to detect DNA. “As received” C6 S-S-ssDNA eluted prior to PEG-MAL (Figure 26). The chromatogram exhibits two peaks, in accordance to PAGE analysis (Figure 13), which showed the presence of two bands, the upper correspondent to the dimeric form of ssDNA (Figure 26 b, peak *dimeric form*) and the lower correspondent to ssDNA (Figure 26 b, peak *ssDNA*).

The products resultant from the functionalization of multi-arm PEG-MAL with ssDNA eluted as four defined peaks as well as a small shoulder: a well-defined peak with elution time matching that attributed to dimeric form of ssDNA (Figure 26 c, peak *dimeric form*), suggesting that SH-ssDNA dimers were formed during the reaction time (4 hours), despite the higher specificity of SH-MAL reaction; a small shoulder with elution

time correspondent to the ssDNA, most possibly correspondent to the non-thiolated ssDNA (Figure 26 c, peak *ssDNA*); three new peaks, with different absorbance intensities eluting prior than PEG-MAL, which, besides indicating the successful functionalization of PEG-MAL, suggest that the PEG-ssDNA conjugates were polydisperse (Figure 26 c, peaks *a, b, c*). Of note, peaks with elution times matching that of PEG-MAL were not detected, suggesting that all PEG-MAL was functionalized.

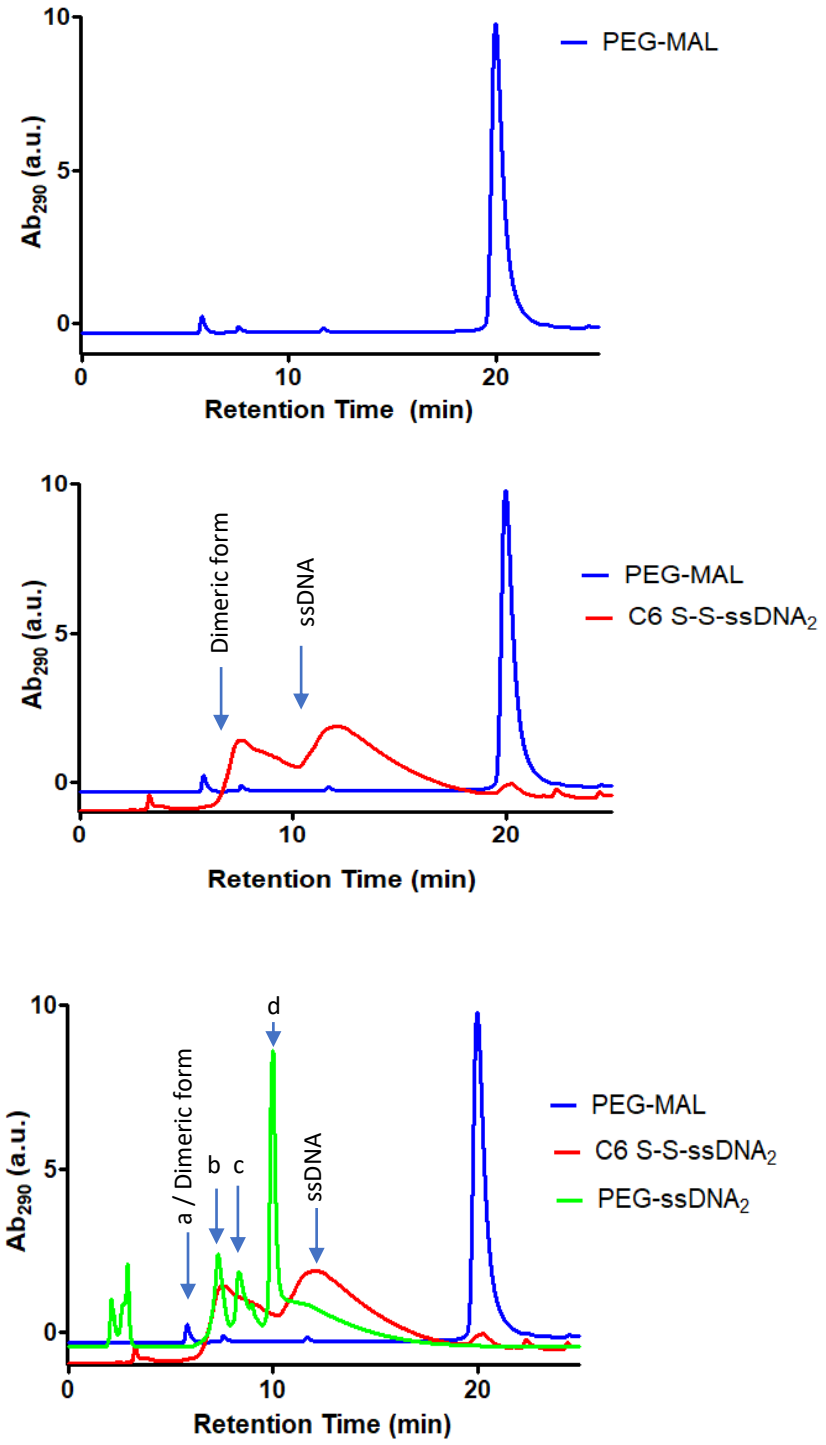

Figure 26. Chromatographic analysis of the formation of PEG-ssDNA conjugates, using a detection wavelength of 290 nm. Figures show representative HPLC chromatograms of: A) PEG (control) B) C6 S-S-ssDNA$_2$ (control); C) Reaction mixture of PEG-MAL with ssDNA$_2$, using a 4:1 SH:PEG-MAL molar ratio. For each condition, the average of 2 chromatograms is shown.

4.3. Analysis of PEG-ssDNA conjugates through gradient-PAGE

The formation of PEG-ssDNA conjugates was further assessed by gradient-PAGE, to support the HPLC results. As this technique requires a smaller amount of sample as compared with HPLC, and due to the high cost of ssDNA, PEG-ssDNA conjugates prepared using different ratios of SH:PEG-MAL (2:1, 4:1 and 6:1) were characterized.

Results are shown in Figure 27. Lanes with PEG-MAL are not shown since this is not detected with SYBR® Gold. In line with HPLC results, bands correspondent to non-thiolated ssDNA and to the dimeric form were detected, mostly for the 4:1 and 6:1 SH:PEG-MAL molar ratios (lanes F4 and F6 in Figure 27). In DTT-reduced C6 S-S-ssDNA the dimeric form is not detected, further supporting that dimers of SH-ssDNA are formed during the 4-hour reaction with PEG-MAL. With the increase of the SH:PEG-MAL molar ratio, three bands became more perceptible, showing the polydispersity of the conjugates, also in accordance to HPLC results.

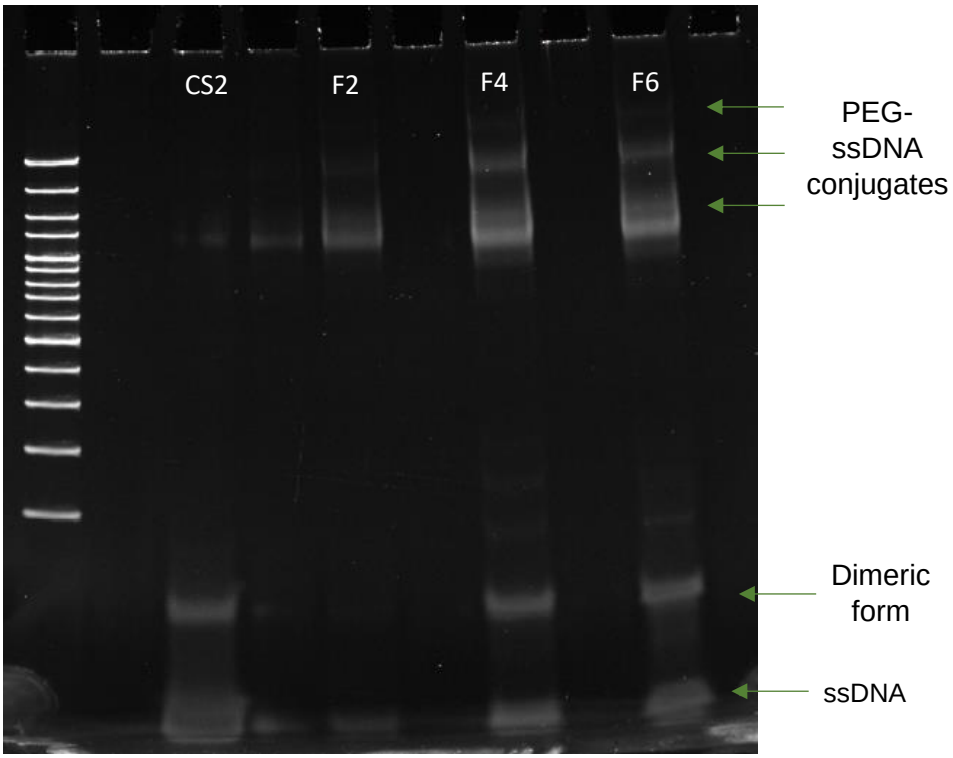

Figure 27. Characterization of PEG-ssDNA conjugates through gradient-PAGE. CS2 corresponds to C6 S-S-ssDNA; F2 corresponds to the molar ratio 2:1 of SH:PEG-MAL; F4 corresponds to the molar ratio 4:1 of SH:PEG-MAL; F6 corresponds to the molar ratio 6:1 of SH:PEG-MAL

4.4. Purification and characterization of PEG-ssDNA conjugates through preparative-SEC

In order to purify and characterize the PEG-ssDNA conjugates, preparative SEC was used. SEC is also a chromatography technique, such as HPLC, where the size of the particles in solution is the key for a good separation, since they can infiltrate the porous column (smaller particle size) or elute immediately (bigger particle size) [128, 129]. It's important to mention that the molecular weight and the size of the molecule don't always correlate [129]. Knowing that three different wavelengths can be used for detection in SEC: 230 nm (star-PEG maximal absorbance), 260 nm (DNA specific absorbance) and 290 nm (MAL specific absorbance) were used. The absorbance spectra for PEG-MAL and ssDNA is provided in Supplementary Information S3.

SEC chromatograms are shown in Figure 28. PEG-MAL showed a single peak while C6 S-S-ssDNA showed two peaks corresponding to different molecular weights, further supporting PAGE and HPLC analysis (Figure 13 and 26). The fractions derived from the reaction mixture showed elution times matching those of the C6 S-S-ssDNA and no peaks correspondent to elution times shorter than PEG-MAL (as expected with the increase of the molecular weight). To clarify these results, fractions were collected and analysed by PAGE (Supplementary Information S4). Since no ssDNA was detected, we concluded that the sample did not enter into the column, possibly due to its increase in the molecular weight, and, as a result, in viscosity.

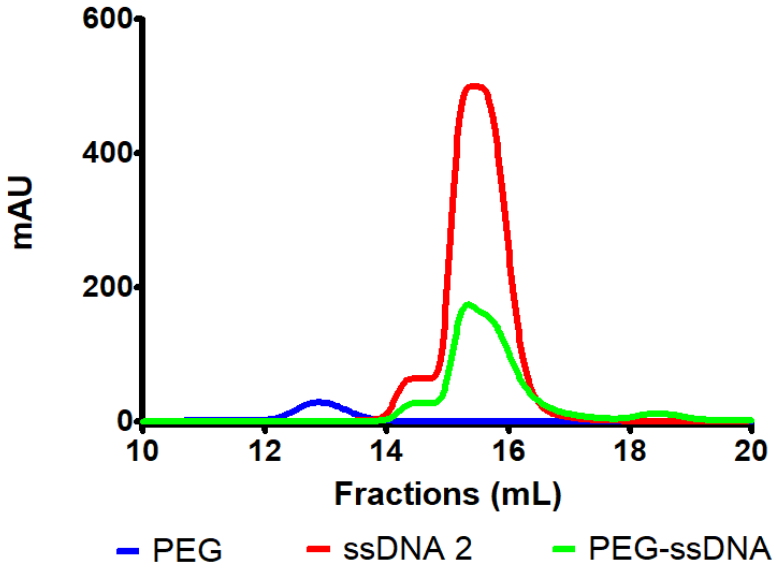

Figure 28. SEC analysis of the PEG-ssDNA conjugates. Figures show representative SEC chromatograms of: Blue) PEG-MAL detected at 230 nm (control); Red) C6 S-S-ssDNA$_2$ detected at 260 nm (control); Green) Reaction mixture of PEG-MAL with ssDNA, using a 4:1 SH:PEG-MAL molar ratio detected at 260 nm. For each condition, the average of 2 chromatograms is shown.

4.5. Purification of PEG-ssDNA conjugates

Since SEC did not allow the separation of PEG-ssDNA conjugates from low molecular weight species, namely from unreacted ssDNA (non-thiolated and dimeric form of ssDNA), diafiltration with Amicon columns 30 kDa was performed (the use of 10 kDa columns showed to be inefficient, Supplementary Information S5).

Results are depicted in Figure 29 and show an apparent reduction in the intensity of the bands correspondent to the non-thiolated ssDNA as well as to that correspondent to the dimeric form of ssDNA. Semi-quantitative analysis of the bands intensity revealed a decrease of the total unreacted ssDNA by almost 50%.

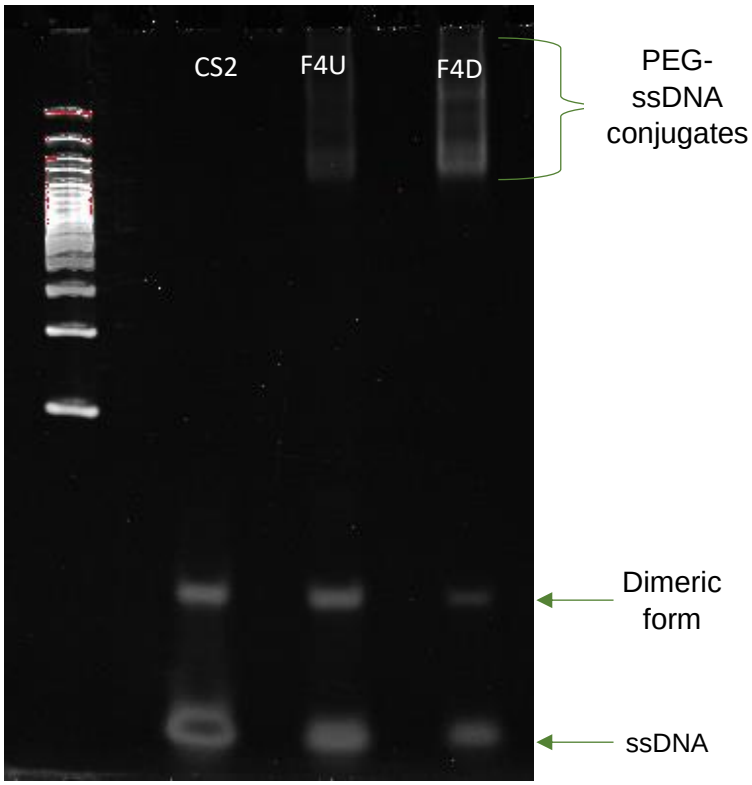

Figure 29. PAGE analysis of the reaction mixture of PEG-MAL with ssDNA, before and after diafiltration with Amicon 30 kDa. PEG-MAL was functionalized using a 4:1 SH:PEG-MAL molar ratio. CS2, represents C6 S-S-DNA; F4U, corresponds to the molar ratio 4:1 of SH:PEG-MAL, unpurified; F4D, corresponds to the molar ratio 4:1 of SH:PEG-MAL, after diafiltration with Amicon 30 kDa

The same image analysis software allowed to detect beside the three bands previously attributed for PEG-ssDNA conjugates, two additional bands in the same region. Subsequent band intensity measurements allowed the estimation of the relative percentage of each PEG-ssDNA conjugate (Figure 30), considering the molar ratio of SH:PEG-MAL (4:1) used. With this specific molar ratio, the prevalent conjugate was not PEG with 4 arms functionalized with ssDNA, but PEG with 2 functionalized arms.

This can be due to conformational changes of PEG-MAL upon the tethering of ssDNA, and its effect on the availability of the remaining MAL reactive groups for binding to ssDNA sequences. Nevertheless, these semi-quantitative results need to be supported by other techniques capable to provide the molecular weight of the conjugates, namely liquid chromatography–mass spectrometry, a technique recently established at i3S. This is a promising technique for the characterization of the present PEG-ssDNA conjugates, since the polar phase of the column is the same as that used in HPLC analysis.

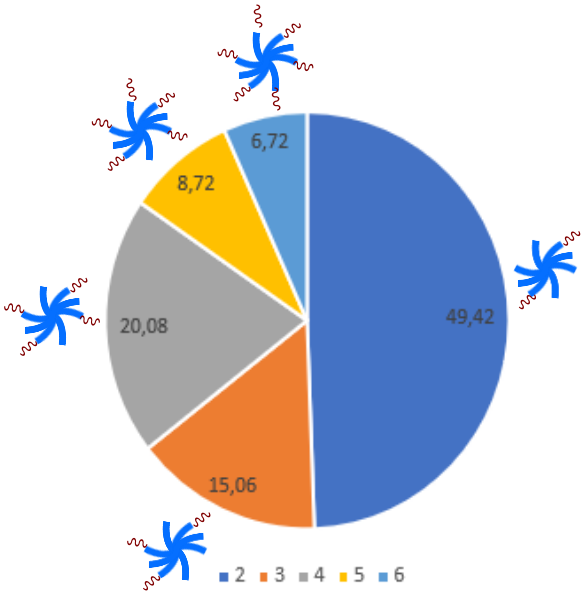

Figure 30. Relative percentage of each PEG-ssDNA conjugate, estimated from the measurement of PAGE band intensities, PEG-MAL arms functionalized with ssDNA, as estimated from semiquantitative analysis of PAGE bands.

5. PEG-RGDS-DNA hydrogels

While the obtention of purified reduced ssDNA was being optimized, DTT-reduced C6 S-S-ssDNA½ purified using MicroSpin G25 columns was used to prepare PEG-RGDS-ssDNA½ conjugates, and their ability to form a hydrogel network assessed, as a proof of concept. For this preliminary assay, PEG-RGDS-ssDNA½ conjugates were prepared using a molar ratio of PEG:RGDS:SH-ssDNA of 1:1:4. The biofunctionalization of a single PEG-MAL arm assured a final concentration of RGDS in the gel of 1.34 mM, which is an RGDS concentration sufficient to support cell viability and neuronal differentiation of neural stem/progenitor cells (NSPC) within 3D hydrogels [130].

The viscoelastic properties of the resultant PEG-RGDS-DNA hydrogels were characterized by dynamic rheology (Figure 31). The hydrogels revealed a low storage modulus (16.64 ± 11.36 Pa), which suggests a low degree of crosslinking. Hydrogels for delivery of NSPC should present stiffness in the range of that of CNS tissues (100 to 1000 Pa), as described in *Introduction*. Moreover, a number of studies have shown that NSPC neuronal differentiation is favoured in soft matrices, namely with associated G' values not higher than 700 Pa [130] and this is the range of stiffness envisaged for PEG-RGDS -DNA hydrogels. The poor mechanical properties observed were attributed to the presence of DTT in the solution of reduced "purified" SH-ssDNA, which, due to its two free thiol groups, most possibly competed with SH-ssDNA for the binding to MAL groups from PEG-MAL. By using DTT-reduced C6 S-S-ssDNA½ purified through Glen GelPak 1.0 mL gravity columns this issue is expected to be overcome.

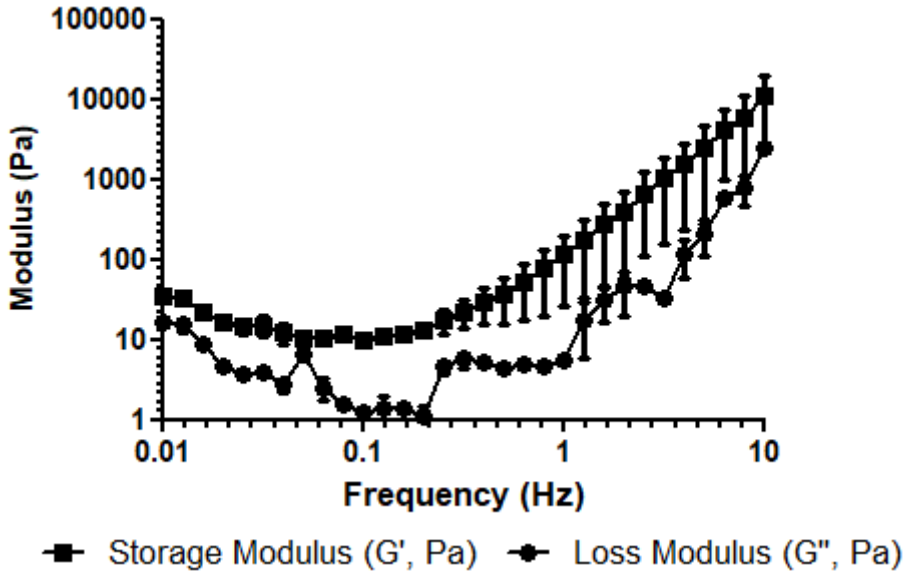

Figure 31. Viscoelastic properties of PEG-RGDS-DNA hydrogels at 37°C, as assessed by oscillatory rheology. The graph denotes the storage and the loss moduli (G' and G‴, respectively) as a function of angular frequency, when imposing a constant strain amplitude of 2% (mean ± SD, n = 4 independent measurements).

A shear thinning assay was performed according Mulyasasmita et al (2014) [51] to assess the shear-thinning properties of the hydrogels. Despite its low stiffness, the PEG-RGDS-DNA hydrogel revealed a shear-thinning and self-healing behaviour, as expected from physically-crosslinked hydrogels (Figure 32).

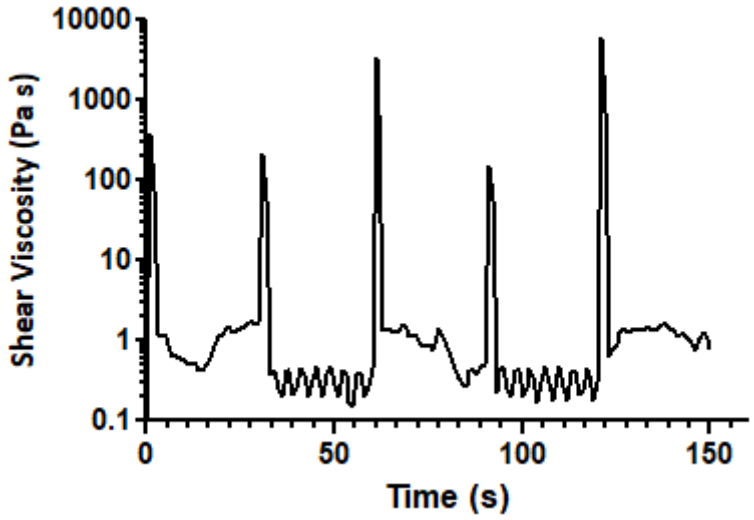

Figure 32. Thixotropic properties of PEG-RGDS-DNA hydrogels at 37°C, as assessed by oscillatory rheology. The graph denotes linear shear viscosity measured under alternating shear rates (0.1 and 10 s−1; 30-s duration). Although the differences between the shear viscosity are small, these suggests a shear-thinning and self-healing behaviour

6. Effect of the combined immobilization of HYD1 and AG73 on NSC neurite outgrowth within fibrin hydrogels

In this study, we also explored the efficacy of the combined immobilization of HYD1 and AG73, two cell adhesive peptides with neurite-promoting ability, in enhancing neurite outgrowth of NSPC in 3D matrices. As PEG-RGDS-DNA hydrogels were still ongoing optimization, these studies were performed using fibrin (Fb) hydrogel as the platform for the 3D culture of NSPC. Due to the modulatory role of syndecans on integrin signalling, the combination of HYD1 (recognized by integrin α6β1) and AG73 (recognized by syndecan-1 and -4) was expected to synergistically increase outward migration of NSPC [131]. In this study we used input peptide concentrations previously optimized for individual peptides in terms of ability to promote neurite outgrowth of H9-derived NSC in Fb hydrogels [89].

Since as the incorporation of an increased amount of peptides could lead to changes in the viscoelastic properties of Fb which could *per se* contribute to the differential cell behaviour observed *in vitro*, HYD1 and AG73-functionalized Fb gels were first characterized in terms of mechanical properties by dynamic rheology. Results are shown in Figure 33. Peptide incorporation did not significantly impact either the G'

(storage modulus) or the G'' (loss modulus) (p = 0.0759 and 0.1132 respectively), in agreement with previous studies reporting minor disruption of fibrin structure during peptide incorporation using the same enzymatic crosslinking approach. In fact, this approach allows the covalent incorporation of peptides into fibrin to sites in the fibrin(ogen) α chain not used for intermolecular fibrinogen cross-linking [132] with retention of biological activity. Even so, the slight decrease in the storage modulus observed for HYD1 and AG73-functionalized Fb suggests that it is less stiff.

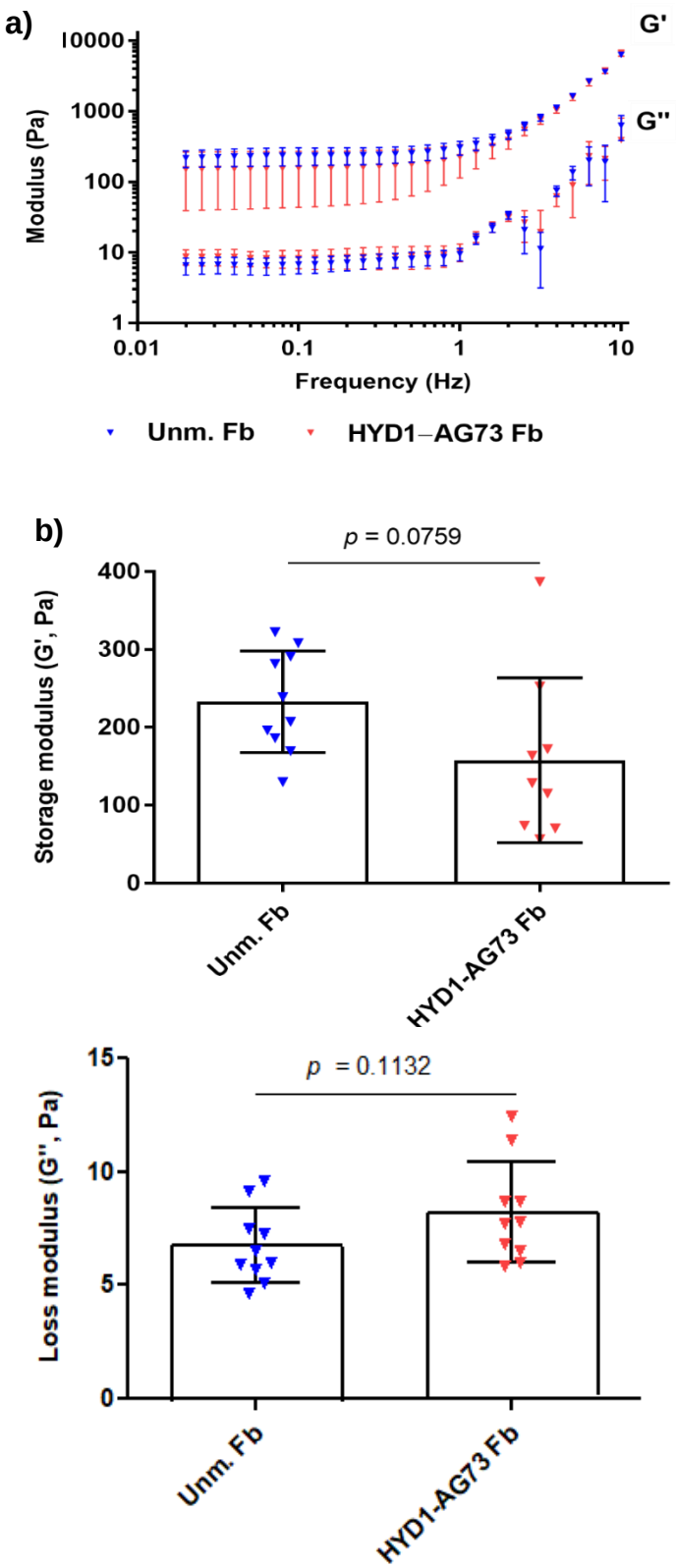

Figure 33. Effect of the combined incorporation of HYD1 (20 μM) and AG73 (60 μM) on the viscoelastic properties of Fb hydrogels, as assessed by oscillatory rheology. a) Storage modulus - G' and loss modulus - G″ as a function of angular frequency, when imposing a constant strain amplitude of 5% (mean ± SD, n = 9-10 independent measurements); b) Storage and c) loss moduli analysed in the frequency range of 0.02 to 0.2 Hz; graphs denote the individual values and the mean ± SD.

H9-derived NSC were seeded as single cells within HYD1 and AG73-functionalized Fb hydrogels and cultured under neuronal differentiation conditions. At day 7 of cell culture, cells were processed for the staining of filamentous actin (F-actin) and DNA. 2D projections of CLSM stack images are presented in Figure 34. Qualitative analysis revealed a similar cell distribution in both unmodified and functionalized hydrogels, and, a tendency to a higher number of neurospheres in the HYD1 and AG73-functionalized gel. Moreover, at a higher magnification, a tendency for higher number of cellular sprouts protruding from the neurospheres was observed in functionalized hydrogels, as compared to unmodified Fb gels. Additional image acquisition and quantitative image analysis are currently undergoing, to support this qualitative analysis.

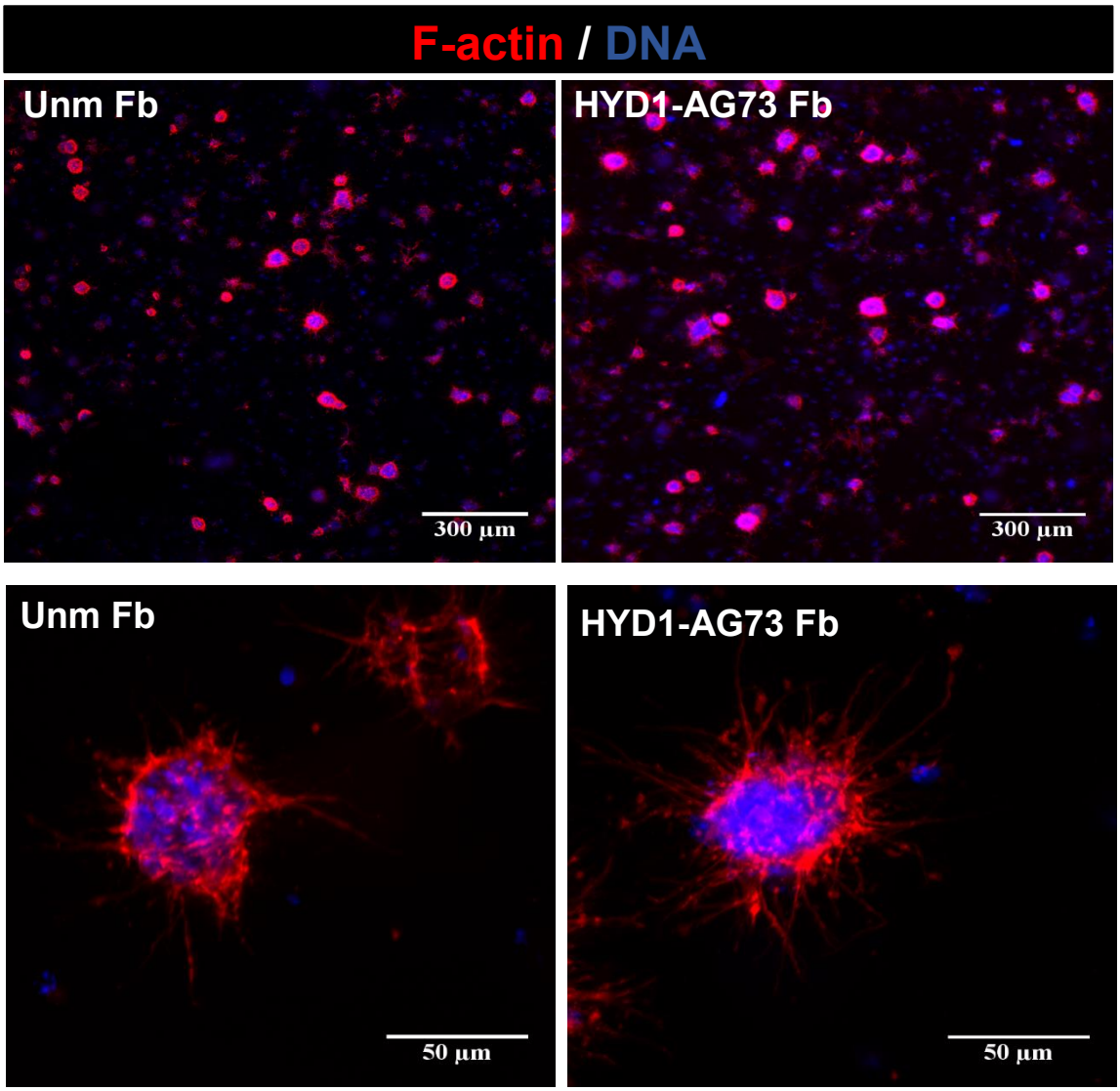

Figure 34. Effect of the combined immobilization of HYD1 and AG73 on H9-NSC neurite outgrowth within fibrin hydrogels. H9-NSC were cultured within unmodified fibrin (Unm Fb) or fibrin functionalized with 20 µM of HYD1 and 60 µM of AG73 (HYD1-AG73 Fb) and processed for F-actin/DNA staining at day 7 of cell culture. Images shown are representative 2D projections of CLSM stack images of the cell matrix constructs.

CHAPTER IV

CONCLUSIONS AND FUTURE PERSPECTIVES

In this study we described the first attempts to develop a fully-defined hydrogel to assist the transplantation of NSPC into the injured CNS, based on DNA self-assembly. The envisaged hydrogel should present bioactivity and compliance to support cell viability and neurite outgrowth of NSPC following transplantation, while presenting shear-thinning and self-healing properties to enable syringe needle injection of cell-carrying hydrogels already in the gel phase, which, besides protecting cells from the mechanical forces experienced during flow [133], can prevent cell dissemination into off-target sites of the CNS.

This was pursued by using 8-arm PEG as the polymer backbone, a pendent RGDS peptide to promote cell adhesion and neurite extension of NSPC, and two complimentary 20nt ssDNA sequences to trigger self-assembling under physiologic conditions.

To allow conjugation with PEG-MAL through SH-MAL addition reaction, the RGSD peptide was synthesized (at GenScript) with a cysteine and ssDNA (at IDT) with a 5' disulfide bond (C6 S-S). While the conjugation of RGDS to PEG-MAL was straightforward that of ssDNA required the prior reduction of the C6 S-S-ssDNA disulfide bond to deprotect the thiol reactive group. Purified reduced SH-ssDNA sequences were successfully obtained after the optimization of the reducing agent and that of the purification columns (to eliminate DTT and to remove or the thiolated by-product C6-SH formed by reduction of disulfide bonds in C6 S-S-ssDNA). Still, the low percentage of reactive thiols in SH-ssDNA, which, dependent on the ssDNA sequence varied from 45 to 76%, is a major hurdle limiting the use of SH-ssDNA for the preparation of PEG-ssDNA conjugates.

The functionalization of PEG-MAL with pendent RGDS groups was performed using different stoichiometric balanced molar ratios of SH groups in RGDS to PEG-MAL, in order to functionalize 1 to 8 arms of the multi-arm PEG. In accordance to the literature, a high incorporation efficiency of RGDS was observed (as high as 95%), as determined quantifying the percentage of remaining free thiol groups in the reaction buffer. Still, further analysis would be necessary to assess the establishment of dimeric forms of RGDS, despite the higher specificity of thiol groups for maleimide groups.

The functionalization of PEG-MAL with pendent SH-ssDNA sequences was performed similarly using different stoichiometric balanced molar ratios of SH groups in SH-ssDNA to PEG-MAL, in order to functionalize 2, 4, or 6 arms of the multi-arm PEG. The analysis of the reaction mixture by gradient PAGE shows the formation of polydisperse PEG-ssDNA conjugates, as also observed by analytical HPLC. Moreover,

for a SH:PEG-MAL molar ratio of 4:1, while the quantification of remaining free thiol groups in the reaction buffer pointed to a high immobilization efficiency of ssDNA (≅ 97%) the analysis of the reaction mixture by analytical HPLC, PAGE, and SEC, suggested the establishment of dimers of SH-ssDNA during the 4-h reaction with PEG-MAL. PEG-ssDNA conjugates could be partially purified using diafiltration columns. However, techniques able to provide the molecular weight of the conjugates such as liquid chromatography-mass spectrometry are needed to further characterize the obtained PEG-ssDNA conjugates. The ability of PEG-RGDS-ssDNA½ conjugates to form a hydrogel network is currently being assessed, as a proof of concept. Still, to overcome the low percentage of reactive thiols in SH-ssDNA as well as the formation of disulfide bonds between SH-ssDNA sequences during the 4-h reaction with PEG-MAL, alternative strategies for the formation of PEG-ssDNA conjugates are currently being considered.

In parallel, while PEG-RGDS-DNA hydrogels were ongoing optimization, we assessed the efficacy of the combined immobilization of HYD1 and AG73, two cell adhesive peptides with neurite-promoting ability, in enhancing neurite outgrowth of NSPC. For this purpose, fibrin hydrogel was used as the platform for the 3D culture of NSC (H9-derived NSC) and functionalized gels prepared at input peptide concentrations previously optimized for individual peptides. We showed that peptide incorporation did not significantly impact either the storage or the loss moduli of fibrin gels. Moreover, qualitative assessment of H9-NSC behaviour revealed a tendency for a higher number of cellular sprouts protruding from the neurospheres in HYD1 and AG73-functionalized hydrogels, as compared to unmodified Fb gels. These promising results need now to be supported by additional image acquisition and quantitative image analysis, to assess if the combination of these peptides has an additive or even a synergistic effect on neurite outgrowth.

REFERENCES

[1] R. Y. Tam, T. Fuehrmann, N. Mitrousis, and M. S. Shoichet, “Regenerative therapies for central nervous system diseases: A biomaterials approach,” *Neuropsychopharmacology*, vol. 39, no. 1, pp. 169–188, 2014.

[2] W. Wang, B. Bu, M. Xie, M. Zhang, Z. Yu, and D. Tao, “Neural cell cycle dysregulation and central nervous system diseases,” *Prog. Neurobiol.*, vol. 89, no. 1, pp. 1–17, 2009.

[3] P. Lu *et al.*, “Long-Distance Growth and Connectivity of Neural Stem Cells after Severe Spinal Cord Injury,” *Cell*, vol. 150, pp. 1264–1273, 2012.

[4] P. J. Horner and F. H. Gage, “Regenerating the damaged central nervous system,” *Nature*, vol. 407, no. 6807, pp. 963–970, 2000.

[5] C. C. Stichel and H. W. Müller, “Experimental strategies to promote axonal regeneration after traumatic central nervous system injury,” *Prog. Neurobiol.*, vol. 56, no. 2, pp. 119–148, 1998.

[6] J. W. Fawcett and R. A. Asher, “The glial scar and central nervous system repair,” *Brain Res. Bull.*, vol. 49, no. 6, pp. 377–391, 1999.

[7] N. Egawa, J. Lok, K. Washida, and K. Arai, “Mechanisms of Axonal Damage and Repair after Central Nervous System Injury,” *Transl. Stroke Res.*, vol. 8, no. 1, pp. 14–21, 2017.

[8] C. Meisel, J. M. Schwab, K. Prass, A. Meisel, and U. Dirnagl, “Central nervous system injury-induced immune deficiency syndrome,” *Nat. Rev. Neurosci.*, vol. 6, no. 10, pp. 775–786, 2005.

[9] R. M. Ransohoff and M. a Brown, “Review series Innate immunity in the central nervous system,” *J. Clin. Invest.*, vol. 122, no. 4, pp. 1164–1171, 2012.

[10] World Health Organization, “Neurological disorders: a public health approach,” *Neurol. Disord. public Heal. challenges.*, vol. 1, pp. 41–176, 2006.

[11] X. Li, E. Katsanevakis, X. Liu, N. Zhang, and X. Wen, “Engineering neural stem cell fates with hydrogel design for central nervous system regeneration,” *Prog. Polym. Sci.*, vol. 37, no. 8, pp. 1105–1129, 2012.

[12] D. Silberberg, N. P. Anand, K. Michels, and R. N. Kalaria, “Brain and other nervous system disorders across the lifespan-global challenges and opportunities,”

Nature, vol. 527, no. 7578, pp. S151–S154, 2015.

[13] A. M. Parr, C. H. Tator, and A. Keating, “Bone marrow-derived mesenchymal stromal cells for the repair of central nervous system injury,” *Bone Marrow Transplant.*, vol. 40, no. 7, pp. 609–619, 2007.

[14] M. E. L. Van Den Berg, J. M. Castellote, I. Mahillo-Fernandez, and J. De Pedro-Cuesta, “Incidence of spinal cord injury worldwide: A systematic review,” *Neuroepidemiology*, vol. 34, pp. 184–192, 2010.

[15] C. Saraiva, C. Praça, R. Ferreira, T. Santos, L. Ferreira, and L. Bernardino, “Nanoparticle-mediated brain drug delivery: Overcoming blood-brain barrier to treat neurodegenerative diseases,” *J. Control. Release*, vol. 235, pp. 34–47, 2016.

[16] M. B. Bracken, M. J. Shepard, W. F. Collins Jr., T. R. Holford, D. S. Baskin, and A. Et, “Methylprednisolone or naloxone treatment after acute spinal cord injury: I-year follow-up data,” *J Neurosurg*, vol. 76, pp. 23–31, 1992.

[17] B. K. Kwon, W. Tetzlaff, J. N. Grauer, J. Beiner, and A. R. Vaccaro, “Pathophysiology and pharmacologic treatment of acute spinal cord injury,” *Spine J.*, vol. 4, no. 4, pp. 451–464, 2004.

[18] F. Han, W. Wang, and C. Chen, “Research progress in animal models and stem cell therapy for Alzheimer ’ s disease,” *J. Neurorestoratology*, vol. 3, pp. 11–22, 2015.

[19] X. M. Xu and S. M. Onifer, “Transplantation-mediated strategies to promote axonal regeneration following spinal cord injury,” *Respir. Physiol. Neurobiol.*, vol. 169, no. 2, pp. 171–182, 2009.

[20] M. M. Pakulska, B. G. Ballios, and M. S. Shoichet, “Injectable hydrogels for central nervous system therapy,” *Biomed. Mater.*, vol. 7, no. 2, pp. 1–14, 2012.

[21] G. I. Mataliotakis and A. Tsirikos, “Spinal cord trauma: classification of spinal cord injury syndromes , treatment principles and controversies,” *Orthopaedics and Trauma*. Elsevier Ltd, pp. 1–10, 2016.

[22] W.-R. Schabitz *et al.*, “Neuroprotective Effect of Granulocyte Colony-Stimulating Factor After Focal Cerebral Ischemia,” *Stroke*, vol. 34, no. 3, pp. 745–751, 2003.

[23] A. L. Vescovi, B. A. Reynolds, D. D. Fraser, and S. Weiss, “bFGF regulates the proliferative fate of unipotent (neuronal) and bipotent (neuronal/astroglial) EGF-generated CNS progenitor cells,” *Neuron*, vol. 11, no. 5, pp. 951–966, 1993.

[24] L. D. F. Moon, R. A. Asher, K. E. Rhodes, and J. W. Fawcett, “Regeneration of CNS axons backto their target following treatment of adult rat brain with chondroitinase ABC,” *Nat. Neurosci.*, vol. 4, no. 5, pp. 465–466, 2001.

[25] T. GrandPré, S. Li, and S. M. Strittmatter, “Nogo-66 receptor antagonist peptide promotes axonal regeneration,” *Lett. to Nat.*, vol. 417, pp. 547–551, 2002.

[26] T. L. Baker-herman *et al.*, “BDNF is necessary and sufficient for spinal respiratory plasticity following intermittent hypoxia,” *Nat. Neurosci.*, vol. 7, no. 1, pp. 48–55, 2004.

[27] T. M. Brushart, P. N. Hoffman, R. M. Royall, B. B. Murinson, C. Witzel, and T. Gordon, “Electrical stimulation promotes motoneuron regeneration without increasing its speed or conditioning the neuron.,” *J. Neurosci.*, vol. 22, no. 15, pp. 6631–6638, 2002.

[28] S. Goldman, “Stem and progenitor cell-based therapy of the human central nervous system,” *Nat. Biotechnol.*, vol. 23, no. 7, pp. 862–871, 2005.

[29] O. Lindvall and Z. Kokaia, “Stem cells in human neurodegenerative disorders — time for clinical translation ?,” *J. Clin. Invest.*, vol. 120, no. 1, p. 29, 2010.

[30] A. R. Bento, P. Quelhas, M. J. Oliveira, A. P. Pêgo, and I. F. Amaral, “Three-dimensional culture of single embryonic stem-derived neural/stem progenitor cells in fibrin hydrogels: neuronal network formation and matrix remodelling,” *J. Tissue Eng. Regen. Med.*, vol. 11, no. 12, pp. 3494–3507, 2017.

[31] J. L. Drury and D. J. Mooney, “Hydrogels for tissue engineering: Scaffold design variables and applications,” *Biomaterials*, vol. 24, no. 24, pp. 4337–4351, 2003.

[32] M. Yousefifard *et al.*, “Neural stem/progenitor cell transplantation for spinal cord injury treatment; A systematic review and meta-analysis,” *Neuroscience*, vol. 322, pp. 377–397, 2016.

[33] H. OKANO, “Neural stem cells and strategies for the regeneration of the central nervous system,” *Proc. Japan Acad. Ser. B*, vol. 86, no. 4, pp. 438–450, 2010.

[34] M. R., “Stem cells in the central nervous system,” *Science (80-.).*, vol. 276\n, no. April, pp. 66–71, 1997.

[35] L. M. Ramer, M. S. Ramer, and E. J. Bradbury, “Restoring function after spinal cord injury: Towards clinical translation of experimental strategies,” *Lancet Neurol.*, vol. 13, no. 12, pp. 1241–1256, 2014.

[36] W. Ma *et al.*, “Three-dimensional collagen gel networks for neural stem cell-based neural tissue engineering,” *Macromol. Symp.*, vol. 227, no. 1, pp. 327–333, 2005.

[37] N. D. Leipzig and M. S. Shoichet, “The effect of substrate stiffness on adult neural stem cell behavior,” *Biomaterials*, vol. 30, no. 36, pp. 6867–6878, 2009.

[38] Y. Tang, P. Yu, and L. Cheng, “Current progress in the derivation and therapeutic application of neural stem cells,” *Cell Death Dis.*, vol. 8, no. 10, p. e3108, 2017.

[39] K. F. Nilsson, “No Title.” [Online]. Available: http://www.igp.uu.se/research/neuro-oncology/karin-forsberg-nilsson/. [Accessed: 09-Aug-2018].

[40] “Clinical Trials.” [Online]. Available: http://clinicaltrials.gov. [Accessed: 24-Feb-2018].

[41] P. Lu *et al.*, “Prolonged human neural stem cell maturation supports recovery in injured rodent CNS,” *J. Clin. Invest.*, vol. 127, no. 9, pp. 3287–3299, 2017.

[42] S.-W. Jeong, K. Chu, K.-H. Jung, S. U. Kim, M. Kim, and J.-K. Roh, “Human Neural Stem Cell Transplantation Promotes Functional Recovery in Rats With Experimental Intracerebral Hemorrhage,” *Stroke*, vol. 34, no. 9, pp. 2258–2263, 2003.

[43] J. M. Zhu, Y. Y. Zhao, S. D. Chen, W. H. Zhang, L. Lou, and X. Jin, “Functional recovery after transplantation of neural stem cells modified by brain-derived neurotrophic factor in rats with cerebral ischaemia,” *J. Int. Med. Res.*, vol. 39, no. 2, pp. 488–498, 2011.

[44] A. M. Parr *et al.*, “Transplanted adult spinal cord-derived neural stem/progenitor cells promote early functional recovery after rat spinal cord injury,” *Neuroscience*, vol. 155, no. 3, pp. 760–770, 2008.

[45] C. Neurosciences Ltd, “OpRegen: A New Treatment for Dry AMD.” [Online]. Available: http://www.cellcureneurosciences.com/our-clinical-. [Accessed: 28-Feb-2018].

[46] O. Therapeutics Inc, “Ocata Therapeutics.” [Online]. Available: https://www.bloomberg.com/research/stocks/private/. [Accessed: 28-Feb-2018].

[47] CHA Biotec, “CHA Biotec.” [Online]. Available: http://en.chabio.com/ir_new_view.asp. [Accessed: 15-Feb-2018].

[48] J. W. Mcdonald *et al.*, “Repair of the Injured Spinal Cord and the Potential of Embryonic Stem Cell Transplantation,” *J. Neurotrauma*, vol. 21, no. 4, pp. 383–

393, 2004.

[49] S. Erceg *et al.*, “Transplanted oligodendrocytes and motoneuron progenitors generated from human embryonic stem cells promote locomotor recovery after spinal cord transection,” *Stem Cells*, vol. 28, no. 9, pp. 1541–1549, 2010.

[50] A. P. Pêgo *et al.*, “Regenerative medicine for the treatment of spinal cord injury: More than just promises?,” *J. Cell. Mol. Med.*, vol. 16, no. 11, pp. 2564–2582, 2012.

[51] M. H. Amer, F. R. A. J. Rose, K. M. Shakesheff, M. Modo, and L. J. White, “Translational considerations in injectable cell-based therapeutics for neurological applications: concepts, progress and challenges,” *Regen. Med.*, vol. 2, pp. 1–13, 2017.

[52] A. S. Hoffman, “Hydrogels for biomedical applications,” *Adv. Drug Deliv. Rev.*, vol. 64, no. SUPPL., pp. 18–23, 2012.

[53] T. R. Hoare and D. S. Kohane, “Hydrogels in drug delivery: Progress and challenges,” *Polymer (Guildf).*, vol. 49, no. 8, pp. 1993–2007, 2008.

[54] H. Wang and S. C. Heilshorn, “Adaptable Hydrogel Networks with Reversible Linkages for Tissue Engineering,” *Adv. Mater.*, vol. 27, pp. 3717–3736, 2015.

[55] J. Zhu, “Design properties of hydrogel tissue-engineering scaffolds,” *Expert Rev. Med. Devices*, vol. 8, no. 5, pp. 607–626, 2011.

[56] W. E. Hennink and C. F. van Nostrum, “Novel crosslinking methods to design hydrogels,” *Adv. Drug Deliv. Rev.*, vol. 64, no. SUPPL., pp. 223–236, 2012.

[57] M. F. Akhtar, M. Hanif, and N. M. Ranjha, “Methods of synthesis of hydrogels … A review,” *Saudi Pharm. J.*, vol. 24, no. 5, pp. 554–559, 2016.

[58] D. R. Nisbet, K. E. Crompton, M. K. Horne, D. I. Finkelstein, and J. S. Forsythe, “Neural tissue engineering of the CNS using hydrogels,” *J. Biomed. Mater. Res. - Part B Appl. Biomater.*, vol. 87, no. 1, pp. 251–263, 2008.

[59] L. M. Marquardt and S. C. Heilshorn, “Design of Injectable Materials to Improve Stem Cell Transplantation,” *Curr. Stem Cell Reports*, vol. 2, no. 3, pp. 207–220, 2016.

[60] B. D. Ulery, L. S. Nair, and C. T. Laurencin, “Biomedical applications of biodegradable polymers,” *J. Polym. Sci. Part B Polym. Phys.*, vol. 49, no. 12, pp. 832–864, 2011.

[61] A. C. Brown and T. H. Barker, “Fibrin-based biomaterials: Modulation of macroscopic properties through rational design at the molecular level,” *Acta Biomater.*, vol. 10, no. 4, pp. 1502–1514, 2014.

[62] Y. Li, J. Rodrigues, and H. Tomás, “Injectable and biodegradable hydrogels: Gelation, biodegradation and biomedical applications,” *Chem. Soc. Rev.*, vol. 41, no. 6, pp. 2193–2221, 2012.

[63] D. Barros, I. F. Amaral, and A. P. Pêgo, “Biomimetic synthetic self-assembled hydrogels for cell transplantation.,” *Curr. Top. Med. Chem.*, vol. 15, no. 13, pp. 1209–26, 2015.

[64] Y. Wu, S. Joseph, and N. R. Aluru, “Effect of Cross-Linking on the Diffusion of Water , Ions , and Small Molecules in Hydrogels Effect of Cross-Linking on the Diffusion of Water , Ions , and Small Molecules in Hydrogels,” *Molecules*, vol. 113, pp. 3512–3520, 2009.

[65] E. A. Phelps *et al.*, “Maleimide cross-linked bioactive PEG hydrogel exhibits improved reaction kinetics and cross-linking for cell encapsulation and in situ delivery,” *Adv. Mater.*, vol. 24, pp. 64–70, 2012.

[66] J. Kim, Y. P. Kong, S. M. Niedzielski, R. K. Singh, A. J. Putnam, and A. Shikanov, “Characterization of the crosslinking kinetics of multi-arm poly(ethylene glycol) hydrogels formed via Michael-type addition,” *Soft Matter*, vol. 12, pp. 2076–2085, 2016.

[67] S. Ahadian *et al.*, “Bioconjugated Hydrogels for Tissue Engineering and Regenerative Medicine,” *Bioconjug. Chem.*, vol. 26, pp. 1984–2001, 2015.

[68] H. Tan, C. Xiao, J. Sun, D. Xiong, and X. Hu, “Biological self-assembly of injectable hydrogel as cell scaffold via specific nucleobase pairing,” *Chem. Commun.*, vol. 48, no. 83, p. 10289, 2012.

[69] X. Kong, Q. Tang, X. Chen, Y. Tu, S. Sun, and Z. Sun, “Polyethylene glycol as a promising synthetic material for repair of spinal cord injury,” *Neural Regen. Res.*, vol. 12, no. 6, pp. 1003–1008, 2017.

[70] D. D. McKinnon, A. M. Kloxin, and K. S. Anseth, “Synthetic hydrogel platform for three-dimensional culture of embryonic stem cell-derived motor neurons,” *Biomater. Sci.*, vol. 1, no. 5, pp. 449–548, 2013.

[71] H. J. Chung and T. G. Park, “Self-assembled and nanostructured hydrogels for drug delivery and tissue engineering,” *Nano Today*, vol. 4, pp. 429–437, 2009.

[72] J. Zhang *et al.*, “Physically associated synthetic hydrogels with long-term covalent stabilization for cell culture and stem cell transplantation,” *Adv. Mater.*, vol. 23, no. 43, pp. 5098–5103, 2011.

[73] W. Mulyasasmita *et al.*, “Avidity-controlled hydrogels for injectable co-delivery of induced pluripotent stem cell-derived endothelial cells and growth factors,” *J. Control. Release*, vol. 191, pp. 71–81, 2014.

[74] C. T. S. Wong Po Foo, J. S. Lee, W. Mulyasasmita, A. Parisi-amon, and S. C. Heilshorn, “Two-component protein-engineered physical hydrogels for cell encapsulation,” *Cell*, vol. 106, no. 52, pp. 22067–22072, 2009.

[75] C. Li *et al.*, “A supramolecular hydrogel with identical cross-linking point density but distinctive rheological properties,” *Mater. Chem. Front.*, vol. 10, pp. 1–6, 2017.

[76] P. Moshayedi *et al.*, “Systematic optimization of an engineered hydrogel allows for selective control of human neural stem cell survival and differentiation after transplantation in the stroke brain,” *Biomaterials*, vol. 105, pp. 145–155, 2016.

[77] Y. Shao, H. Jia, T. Cao, and D. Liu, “Supramolecular Hydrogels Based on DNA Self-Assembly,” *Acc. Chem. Res.*, vol. 50, pp. 659–668, 2017.

[78] Z. G. Wang and B. Ding, “DNA-based self-assembly for functional nanomaterials,” *Adv. Mater.*, vol. 10, pp. 1–10, 2013.

[79] F. X. Jiang, B. Yurke, B. L. Firestein, and N. A. Langrana, “Neurite outgrowth on a DNA crosslinked hydrogel with tunable stiffnesses,” *Ann. Biomed. Eng.*, vol. 36, no. 9, pp. 1565–1579, 2008.

[80] B. Yurke, “Mechanical Properties of a Reversible, DNA-Crosslinked Polyacrylamide Hydrogel,” *J. Biomech. Eng.*, vol. 126, no. 1, p. 104, 2004.

[81] F. X. Jiang, B. Yurke, D. Verma, M. Previtera, R. Schloss, and N. A. Langrana, “Development of DNA Based Active Macro– Materials for Biology and Medicine: A Review,” *Intech open*, vol. 2, p. 64, 2018.

[82] G. Sicilia *et al.*, “Programmable polymer-DNA hydrogels with dual input and multiscale responses,” *Biomater. Sci.*, vol. 2, no. 2, pp. 203–211, 2014.

[83] F. X. Jiang, B. Yurke, R. S. Schloss, B. L. Firestein, and N. a Langrana, “Effect of dynamic stiffness of the substrates on neurite outgrowth by using a DNA-crosslinked hydrogel.,” *Tissue Eng. Part A*, vol. 16, no. 6, pp. 1873–1889, 2010.

[84] Y. Wang *et al.*, “Constructing Tissue like Complex Structures Using Cell-Laden

DNA Hydrogel Bricks," *ACS Appl. Mater. Interfaces*, vol. 9, no. 14, pp. 12311–12315, 2017.

[85] K. J. Lampe and S. C. Heilshorn, "Building stem cell niches from the molecule up through engineered peptide materials," *Neurosci. Lett.*, vol. 519, no. 2, pp. 138–146, 2012.

[86] M. D. Pierschbacher and E. Ruoslahti, "Cell attachment activity of fibronectin can be duplicated by small synthetic fragments of the molecule," *Nature*, vol. 309, no. 5963, pp. 30–33, 1984.

[87] K. H. Smith, E. Tejeda-Montes, M. Poch, and A. Mata, "Integrating top-down and self-assembly in the fabrication of peptide and protein-based biomedical materials," *Chem. Soc. Rev.*, vol. 40, no. 9, pp. 4563–4577, 2010.

[88] J. Silva *et al.*, "Fibrin functionalization with synthetic adhesive ligands interacting with α6β1 integrin receptor enhance neurite outgrowth of embryonic stem cell-derived neural stem/progenitors," *Acta Biomater.*, vol. 59, pp. 243–256, 2017.

[89] A. R. Bento, "Improving neurite outgrowth in 3D hydrogel matrices by mimicking cell receptor-ECM interactions occurring in neurogenic niches: an engineering approach to develop more efficient neural stem cell hydrogel carriers," PhD Thesis, FEUP, 2018.

[90] J. C. Schense, J. Bloch, P. Aebischer, and J. A. Hubbell, "Enzymatic incorporation of bioactive peptides into fibrin matrices enhances neurite extension," *Nat. Biotechnol.*, vol. 18, no. 4, pp. 415–419, 2000.

[91] M. Hiraoka, K. Kato, T. Nakaji-Hirabayashi, and H. Iwata, "Enhanced survival of neural cells embedded in hydrogels composed of collagen and laminin-derived cell adhesive peptide," *Bioconjug. Chem.*, vol. 20, no. 5, pp. 976–983, 2009.

[92] Y. Yamada, K. Hozumi, F. Katagiri, Y. Kikkawa, and M. Nomizu, "Biological activity of laminin peptide-conjugated alginate and chitosan matrices.," *Biopolymers*, vol. 94, no. 6, pp. 711–720, 2010.

[93] Y. Yamada, F. Katagiri, K. Hozumi, Y. Kikkawa, and M. Nomizu, "Cell behavior on protein matrices containing laminin α1 peptide AG73," *Biomaterials*, vol. 32, no. 19, pp. 4327–4335, 2011.

[94] Y. Luo and M. S. Shoichet, "A photolabile hydrogel for guided three-dimensional cell growth and migration," *Nat. Mater.*, vol. 3, no. 4, pp. 249–253, 2004.

[95] K. Saha *et al.*, “Substrate modulus directs neural stem cell behavior,” *Biophys. J.*, vol. 95, no. 9, pp. 4426–4438, 2008.

[96] J. C. Schense and J. A. Hubbell, “Cross-linking exogenous bifunctional peptides into fibrin gels with factor XIIIa,” *Bioconjug. Chem.*, vol. 10, no. 1, pp. 75–81, 1999.

[97] H. J. Lim *et al.*, “Human Induced Pluripotent Stem Cell Derived Neural Stem Cell Survival and Neural Differentiation on Polyethylene Glycol Dimethacrylate Hydrogels Containing a Continuous Concentration Gradient of *N* -Cadherin Derived Peptide His-Ala-Val-Asp-Ile,” *ACS Biomater. Sci. Eng.*, vol. 3, no. 5, pp. 776–781, 2017.

[98] F. Gelain, D. Bottai, A. Vescovi, and S. Zhang, “Designer self-assembling peptide nanofiber scaffolds for adult mouse neural stem cell 3-dimensional cultures,” *PLoS One*, vol. 1, no. 1, pp. 1–11, 2006.

[99] S. Koutsopoulos and S. Zhang, “Long-term three-dimensional neural tissue cultures in functionalized self-Assembling peptide hydrogels, Matrigel and Collagen i,” *Acta Biomater.*, vol. 9, no. 2, pp. 5162–5169, 2013.

[100] C. S. Ahuja and M. Fehlings, “Concise Review: Bridging the Gap: Novel Neuroregenerative and Neuroprotective Strategies in Spinal Cord Injury,” *Stem Cells Transl. Med.*, vol. 5, no. 7, pp. 914–924, 2016.

[101] M. Guvendiren, H. D. Lu, and J. A. Burdick, “Shear-thinning hydrogels for biomedical applications,” *Soft Matter*, vol. 8, no. 2, pp. 260–272, 2012.

[102] H. D. Lu, M. B. Charati, I. L. Kim, and J. A. Burdick, “Injectable shear-thinning hydrogels engineered with a self-assembling Dock-and-Lock mechanism,” *Biomaterials*, vol. 33, pp. 2145–2153, 2012.

[103] A. C. Gaffey *et al.*, “Injectable shear-thinning hydrogels used to deliver endothelial progenitor cells, enhance cell engraftment, and improve ischemic myocardium,” *J. Thorac. Cardiovasc. Surg.*, vol. 150, no. 5, pp. 1268–1276, 2015.

[104] J. N. Zadeh *et al.*, “NUPACK: Analysis and Design of Nucleic Acid Systems JOSEPH,” *J. Comput. Chem.*, vol. 30, no. 10, pp. 1545–1614, 2009.

[105] IDT, “Use thiol modifications to prepare synthetic oligos for attachment chemistry.” [Online]. Available: https://eu.idtdna.com/pages/education/decoded/article/use-thiol-modifications-to-prepare-synthetic-oligos-for-attachment-chemistry. [Accessed: 05-Aug-2018].

[106] T. Information, “Micro Bio-Spin ® Chromatography Columns,” *Molecules*. pp. 6–7, 2018.

[107] GE Healthcare, “illustra MicroSpin Columns User Manual,” *Prod. Bookl.*, vol. 01, pp. 1–23, 2006.

[108] G. Research, “DNA and RNA Desalting,” *Glen Gel-Pak ™ Cartridges*, vol. 1.5.1. pp. 1–6, 2013.

[109] Q. Facts, “Measure-iT ™ Thiol Assay Kit (M30550),” *Product Information*. pp. 1–5, 2008.

[110] M. V. Tsurkan *et al.*, “Defined polymer-peptide conjugates to form cell-instructive starpeg-heparin matrices in situ,” *Adv. Mater.*, vol. 25, no. 18, pp. 2606–2610, 2013.

[111] Sigma-Aldrich, “Protocol for Thiol-Modified Oligonucleotide Reduction Definitions / Abbreviations.” .

[112] G. T. Hermanson, “The Reactions of Bioconjugation,” in *Bioconjugate Techniques*, 2013, pp. 229–258.

[113] G. T. Hermanson, “Functional Targets for Bioconjugation,” in *Bioconjugate Techniques*, 2013, pp. 127–228.

[114] A. M. Faucher and C. Grand-Maître, “Tris(2-Carboxyethyl)phosphine (TCEP) for the reduction of sulfoxides, sulfonylchlorides, N-oxides, and azides,” *Synth. Commun.*, vol. 33, no. 20, pp. 3503–3511, 2003.

[115] bio SYNTHESIS, “Instruction of reduction reaction using TCEP,” *Bio Synthesis*. pp. 1–2, 2018.

[116] B. Bestas *et al.*, “Design and Application of Bispecific Splice-Switching Oligonucleotides,” *Nucleic Acid Ther.*, vol. 24, no. 1, pp. 13–24, 2014.

[117] D. E. Shafer, J. K. Inman, and A. Lees, “Reaction of tris(2-carboxyethyl)phosphine (TCEP) with maleimide and α- haloacyl groups: Anomalous elution of TCEP by gel filtration,” *Anal. Biochem.*, vol. 282, no. 1, pp. 161–164, 2000.

[118] D. T. T. Dithiothreitol, “DTT (DithioThreitol),” *Prod. Inf.*, vol. 054721, no. 284251, pp. 6–8, 1993.

[119] F. Yang, “Surface Dynamics of a DNA Loop Formation Using Surface Plasmon Resonance,” Faculty of Auburn University, 2015.

[120] A. Seo, J. L. Jackson, J. V. Schuster, and D. Vardar-Ulu, “Using UV-absorbance of intrinsic dithiothreitol (DTT) during RP-HPLC as a measure of experimental redox potential in vitro,” *Anal. Bioanal. Chem.*, vol. 405, no. 19, pp. 6379–6384, 2013.

[121] M. Cindrić *et al.*, “Determination of dithiothreitol in complex protein mixturesbyHPLC-MS,” *J. Sep. Sci.*, vol. 31, no. 20, pp. 3489–3496, 2008.

[122] C. E. Vrentas, S. Onstot, and E. M. Nicholson, “A comparative analysis of rapid methods for purification and refolding of recombinant bovine prion protein,” *Protein Expr. Purif.*, vol. 82, no. 2, pp. 380–388, 2012.

[123] “Introduction to Thiol Modification and Detection—Section 2.1.” [Online]. Available: http://www.thermofisher.com/pt/en/home/references/molecular-probes-the-handbook/thiol-reactive-probes/introduction-to-thiol-modification-and-detection.html. [Accessed: 02-Sep-2018].

[124] D. Tarus *et al.*, “Design of Hyaluronic Acid Hydrogels to Promote Neurite Outgrowth in Three Dimensions,” *ACS Appl. Mater. Interfaces*, vol. 8, no. 38, pp. 25051–25059, 2016.

[125] M. P. Schwartz *et al.*, “Human pluripotent stem cell-derived neural constructs for predicting neural toxicity,” *Proc. Natl. Acad. Sci.*, vol. 112, no. 40, pp. 12516–12521, 2015.

[126] R. O. Hynes, “Integrins: Bidirectional, allosteric signaling machines,” *Cell Press*, vol. 110, no. 6, pp. 673–687, 2002.

[127] B. H. Northrop, S. H. Frayne, and U. Choudhary, “Thiol-maleimide ‘click’ chemistry: Evaluating the influence of solvent, initiator, and thiol on the reaction mechanism, kinetics, and selectivity,” *Polym. Chem.*, vol. 6, no. 18, pp. 3415–3430, 2015.

[128] L. M. L. Nollet, “Fundamentals of HPLC,” 2012.

[129] K. Noach, “Introduction to HPLC.,” *Boll. Chim. Farm.*, vol. 115, no. 10, pp. 671–679, 1976.

[130] J. Lam, S. T. Carmichael, W. E. Lowry, and T. Segura, “Design of experiments methodology to optimize hydrogel for iPSC-NPC culture,” *Adv Heal. Mater*, vol. 4, no. 4, pp. 534–539, 2015.

[131] M. R. Morgan, M. J. Humphries, and M. D. Bass, “Synergistic control of cell

adhesion by integrins and syndecans," *Nat. Rev. Mol. Cell Biol.*, vol. 8, no. 12, pp. 957–969, 2007.

[132] N. A. S Kimura, "Cross-linking Site in Fibrinogen for alpha 2- Plasmin Inhibitor," *J. Biol. Chem.*, vol. 261, no. 33, pp. 15591–15595, 1986.

[133] B. A. Aguado, W. Mulyasasmita, J. Su, K. J. Lampe, and S. C. Heilshorn, "Improving Viability of Stem Cells During Syringe Needle Flow Through the Design of Hydrogel Cell Carriers," *Tissue Eng. Part A*, vol. 18, no. 7–8, pp. 806–815, 2012.

Supplementary Information

S1

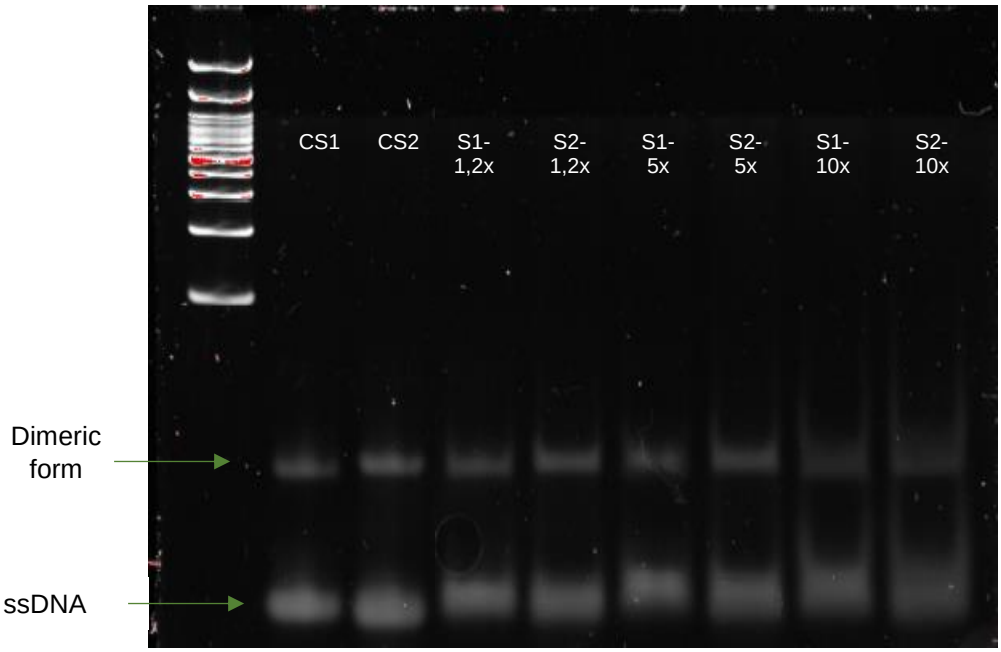

Figure S1. PAGE of the two C6 S-S-ssDNA sequences with TCEP reduction. CS1 and CS2 show C6 S-S-ssDNA sequence 1 and 2, respectively (controls); S1-1,2× and S2-1,2× corresponds C6 S-S-ssDNA 1 and 2, respectively, with 1,2× molar excess of TCEP; S1-5× and S2-5× corresponds C6 S-S-ssDNA 1 and 2, respectively, with 5× molar excess of TCEP; S1-10× and S2-10× corresponds C6 S-S-ssDNA 1 and 2, respectively, with 10× molar excess of TCEP

S2

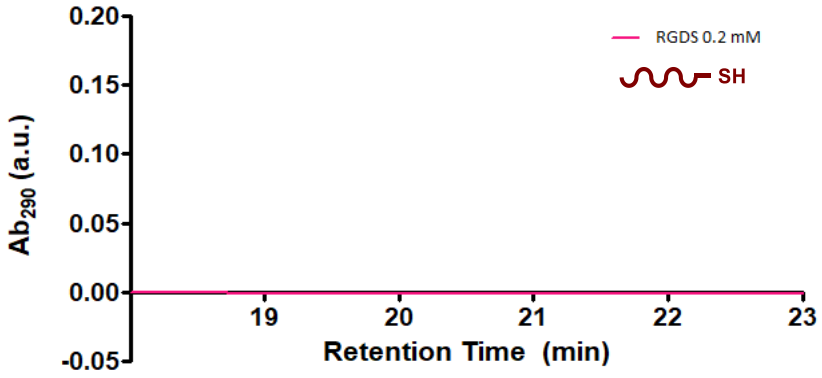

Figure S2. HPLC result for 0.2 mM of RGDS at 290 nm. It is possible to see a that it is not detected at this wavelength.

S3

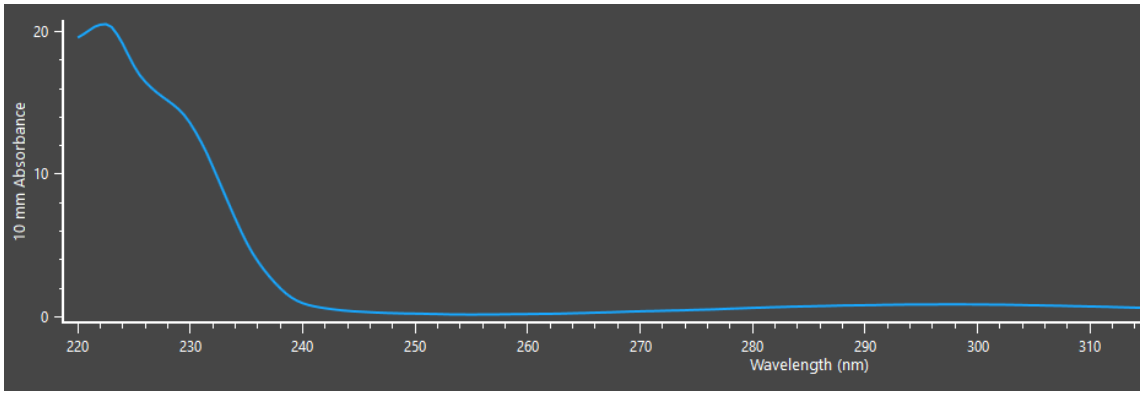

Figure S3 a. Spectrum of PEG-MAL. There is a high value of absorbance at 220 nm, corresponding to the absorbance of PEG, and small peak at 290 nm corresponding to the absorbance of the MAL's present. Spectrum taken with NanoDrop™ One Microvolume UV-Vis spectrophotometer (Termo Fischer) and analysed with Nanodrop™ One Viewer.

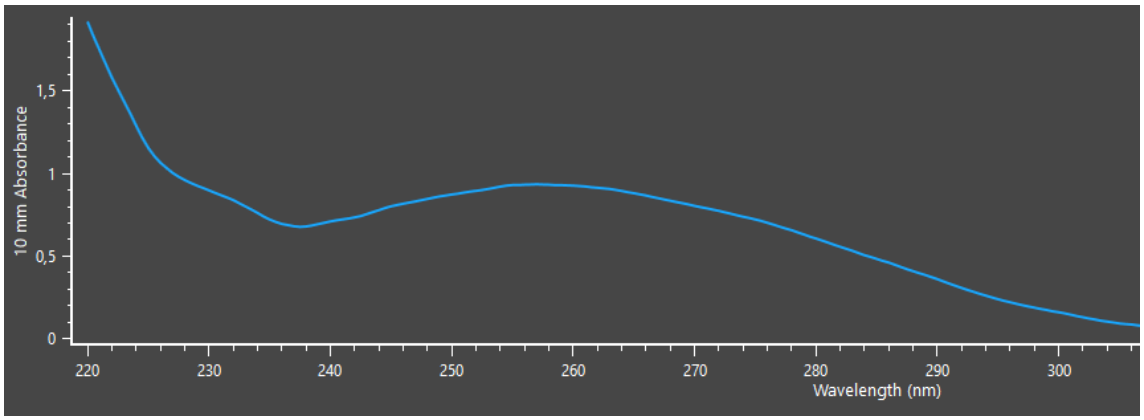

Figure S3 b. Typical spectrum of ssDNA ½. There is a high absorbance peak at 260 nm correspondent the oligonucleotides. The concentration of the sample can be measured by this value divided by the ext. coefficient. Spectrum taken with NanoDrop™ One Microvolume UV-Vis spectrophotometer (Termo Fischer) and analysed with Nanodrop™ One Viewer.

S4

Figure S4. PAGE with PEG-MAL functionalized ssDNA ½ fractions recovered from the SEC assay. It is possible to verify, near the wells, that the sample was charged, however, no DNA was present. Corroborating the fact that the sample did not enter the column.

S5

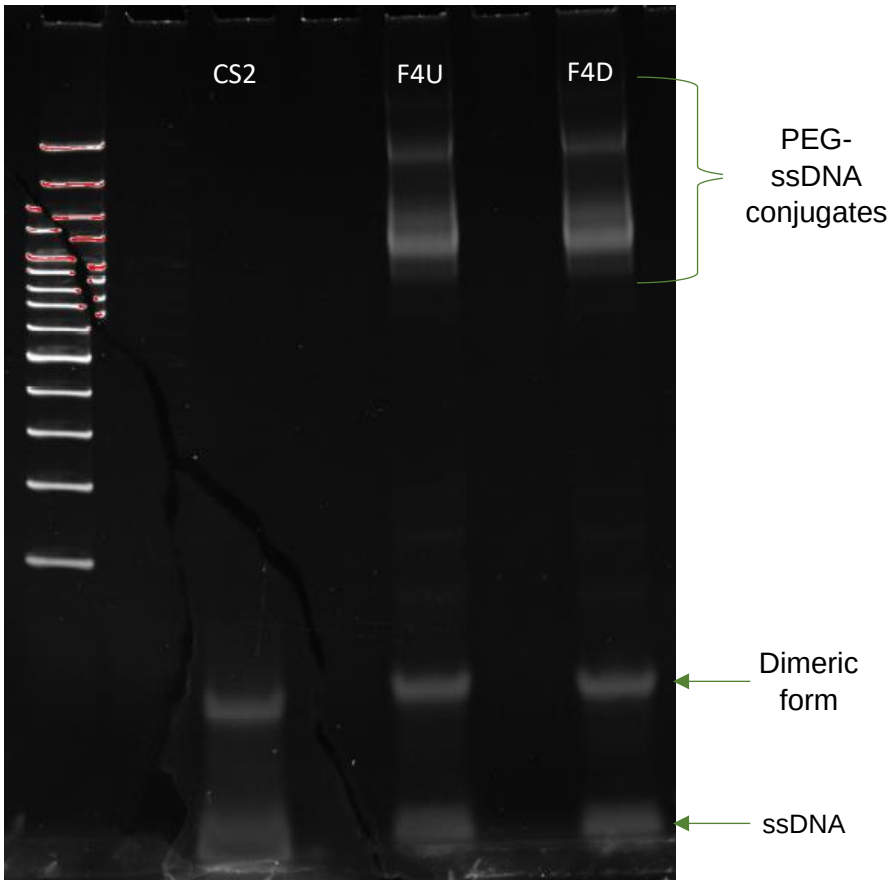

Figure S5. PAGE analysis of the reaction mixture of PEG-MAL with ssDNA, before and after diafiltration with Amicon 10 kDa. PEG-MAL was functionalized using a 4:1 SH:PEG-MAL molar ratio. CS2, represents C6 S-S-DNA; F4U, corresponds to the molar ratio 4:1 of SH:PEG-MAL, unpurified; F4D, corresponds to the molar ratio 4:1 of SH:PEG-MAL, after diafiltration with Amicon 10 kDa